AD-A120 648 MSW VARIABLE TIME-DELAY TECHNIQUES(U) WESTINGHOUSE ELECTRIC CORP PITTSBURGH PA J D ADAM ET AL. JUL 82 81-6F3-DELAY-R4 RADC-TR-82-206 F19628-80-C-0150 1/1

UNCLASSIFIED F/G 20/2 NL

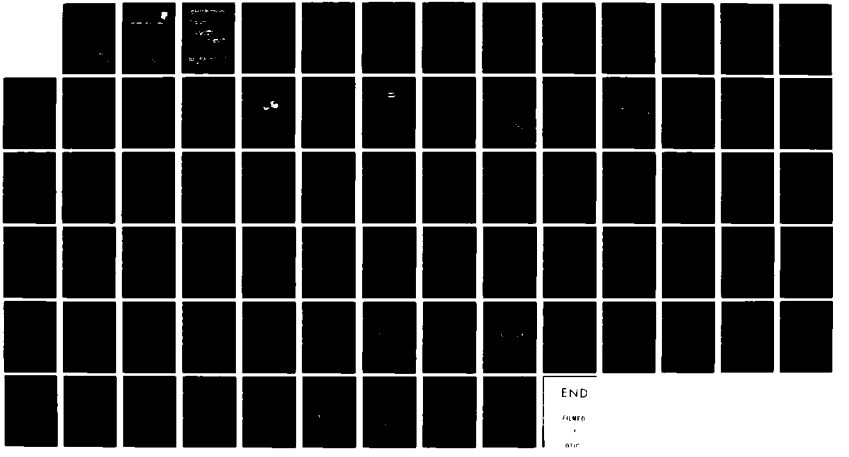

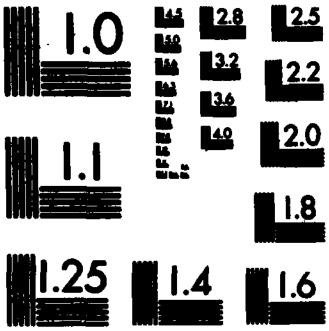

MICROCOPY RESOLUTION TEST CHART
NATIONAL BUREAU OF STANDARDS-1963-A

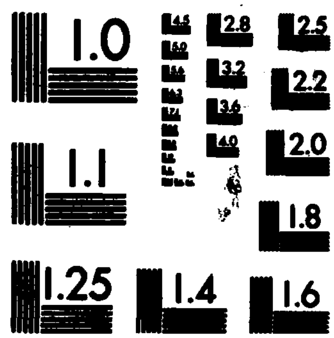

MICROCOPY RESOLUTION TEST CHART
NATIONAL BUREAU OF STANDARDS-1963-A

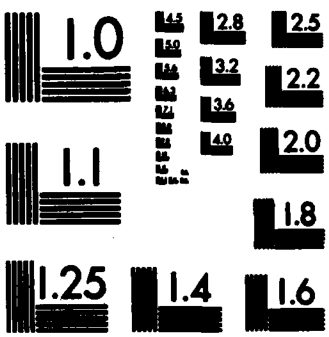

MICROCOPY RESOLUTION TEST CHART
NATIONAL BUREAU OF STANDARDS-1963-A

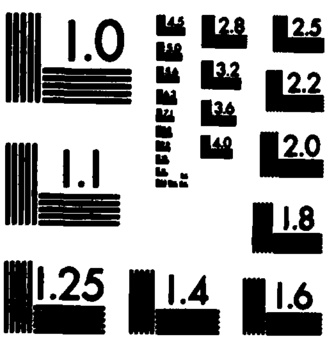

MICROCOPY RESOLUTION TEST CHART
NATIONAL BUREAU OF STANDARDS-1963-A

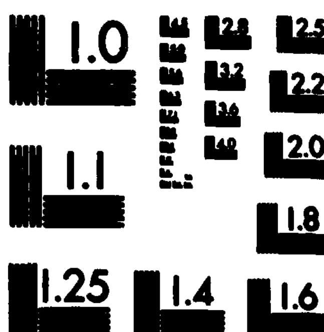

MICROCOPY RESOLUTION TEST CHART
NATIONAL BUREAU OF STANDARDS-1963-A

RADC-TR-82-206
Interim Report
July 1982

MSW VARIABLE TIME-DELAY TECHNIQUES

Westinghouse Electric Corporation

J. D. Adam, M. R. Daniel, P. R. Emtage and R. W. Weinert

ROME AIR DEVELOPMENT CENTER
Air Force Systems Command
Griffiss Air Force Base, NY 13441

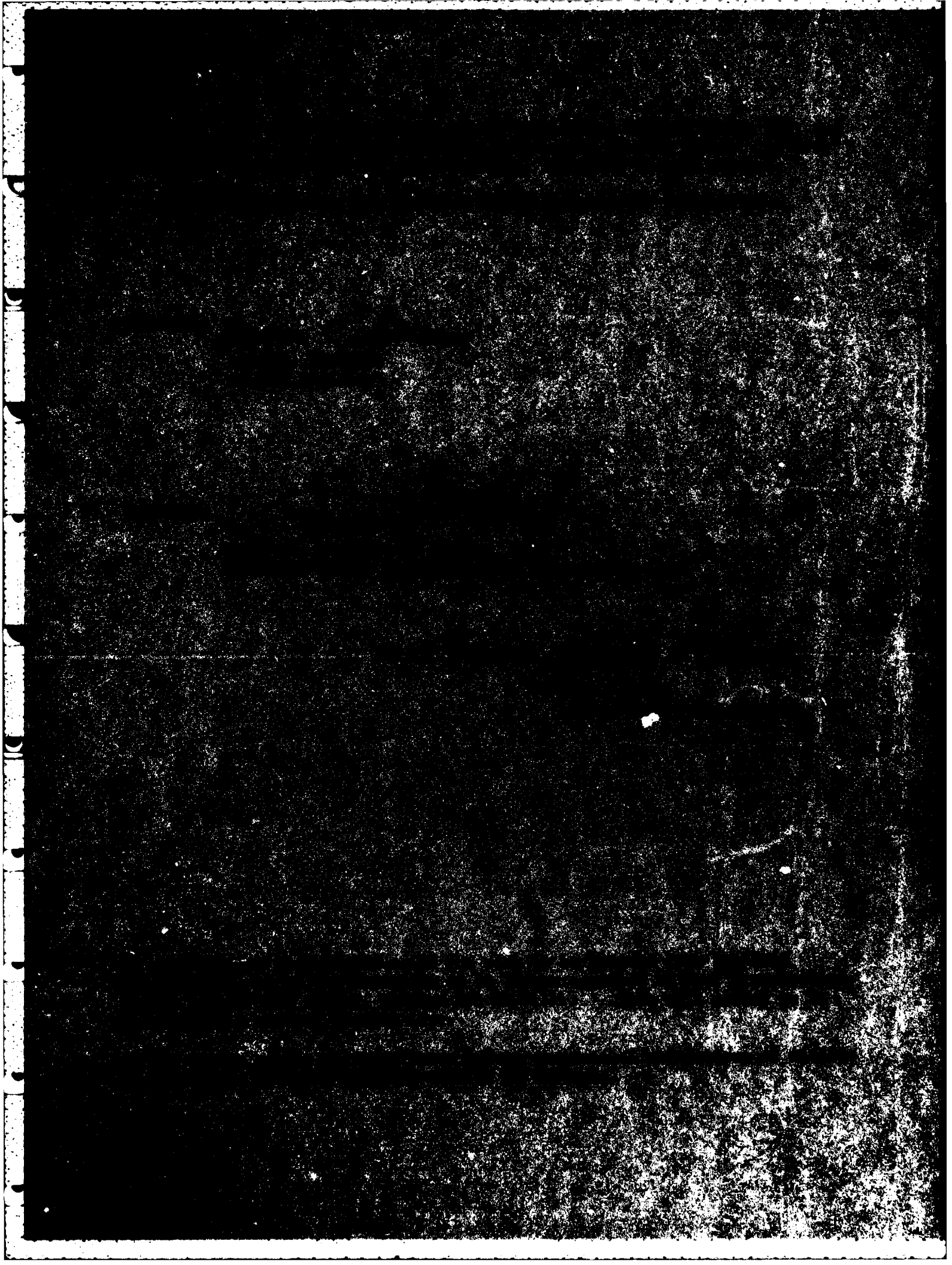

UNCLASSIFIED

SECURITY CLASSIFICATION OF THIS PAGE (When Data Entered)

REPORT DOCUMENTATION PAGE	READ INSTRUCTIONS BEFORE COMPLETING FORM
1. REPORT NUMBER: RADC-TR-82-206	2. GOVT ACCESSION NO: AD-A120 648
	3. RECIPIENT'S CATALOG NUMBER
4. TITLE (and Subtitle): MSW VARIABLE TIME-DELAY TECHNIQUES	5. TYPE OF REPORT & PERIOD COVERED: Interim Report 1 Aug 80 - 30 Sep 81
	6. PERFORMING ORG. REPORT NUMBER: 81-6F3-DELAY-R4
7. AUTHOR(s): J.D. Adam, P.R. Emtage, M.R. Daniel, R.W. Weinert	8. CONTRACT OR GRANT NUMBER(s): F19628-80-C-0150
9. PERFORMING ORGANIZATION NAME AND ADDRESS: Westinghouse Electric Corporation, 1310 Beulah Road, Pittsburgh PA 15232	10. PROGRAM ELEMENT, PROJECT, TASK AREA & WORK UNIT NUMBERS: 61102F, 2305J529
11. CONTROLLING OFFICE NAME AND ADDRESS: Rome Air Development Center (EEAC), Hanscom AFB MA 01731	12. REPORT DATE: July 1982
	13. NUMBER OF PAGES: 80
14. MONITORING AGENCY NAME & ADDRESS(if different from Controlling Office): Same	15. SECURITY CLASS. (of this report): UNCLASSIFIED
	15a. DECLASSIFICATION/DOWNGRADING SCHEDULE: N/A

16. DISTRIBUTION STATEMENT (of this Report)

Approved for public release; distribution unlimited

17. DISTRIBUTION STATEMENT (of the abstract entered in Block 20, if different from Report)

Same

18. SUPPLEMENTARY NOTES

RADC Project Engineer: James C. Sethares (EEAC)

19. KEY WORDS (Continue on reverse side if necessary and identify by block number)

Magnetostatic	Phase	Measurements
Delay	Dispersion	Angle
YIG	Epitaxy	
Microwaves	Films	

20. ABSTRACT (Continue on reverse side if necessary and identify by block number)

Work performed during the first year of a program to investigate magnetostatic wave device techniques for phased arrays and microwave signal processing is described. Among the topics covered is a variable delay line formed by a backward volume wave "down-chirp" and a forward volume wave "up-chirp"; propagation in YIG films biased at an arbitrary angle; propagation and transduction in double YIG films; and the growth of Sm-doped GGG suitable for use as an epitaxial spacer between two YIG films.

DD FORM 1 JAN 73 1473 EDITION OF 1 NOV 65 IS OBSOLETE

UNCLASSIFIED

SECURITY CLASSIFICATION OF THIS PAGE (When Data Entered)

TABLE OF CONTENTS

LIST OF FIGURES

1. INTRODUCTION

This report describes work performed in the first year of a program to investigate magnetostatic wave device techniques for phased antenna arrays and microwave signal processing. At the start of this program, initial experiments on variable delay[1] and also broadband linearly dispersive delay[2] using magnetostatic wave delay lines had been demonstrated. Both of these device characteristics have a potentially wide application in radar and ECM systems. However, these magnetostatic wave devices had significant phase error (>100°) which reduced their allure. Thus, the main thrust of this program is to reduce the phase error to less than 10°, which is typically required for devices in radar and ECM systems.

Work on magnetostatic wave delay lines using single YIG films has shown geometries which yield minimum phase errors for both backward-volume wave (BVW) and forward-volume wave (FVW) propagation. An "up-chirp" FVW device and a matching "down-chirp" BVW device have been designed which, when operated in cascade, will give constant but adjustable delay. This is described further in Section 2.1. Magnetostatic wave propagation in a YIG film magnetized in an arbitrary direction is also under investigation. Here the aim is to search for conditions that will yield either linearly dispersive delay characteristics with low phase error or else delay which can be adjusted by the field angle. This work is discussed in Section 2.2.

Devices based on a single YIG film with one or two ground planes have limitations as to the minimum phase error that can be achieved. In addition, the presence of the ground plane results in an increased loss,[2] particularly when the ground plane is close to the YIG film. For this reason, FVW and BVW propagation in double YIG films has been

investigated. A good theoretical understanding of propagation in double films has been achieved and initial studies have been performed on transduction. Experiments have been conducted with YIG films which are separated by a gold wire transducer, and results obtained are in good agreement with calculations. This is described in Section 2.3. An attractive double YIG film geometry is formed by a YIG-GGG-YIG layer structure grown epitaxially on a GGG substrate. The growth of epitaxial Sm-doped GGG is described in Section 2.4.

2. CONSTANT DELAY LINES

2.1 Magnetostatic Wave Delay Lines in Phased Arrays

Variable magnetostatic wave delay lines are potentially useful in phased-array antennas because of the wide instantaneous bandwidth obtained when real time delay, as opposed to phaseshift with a limited 0-2π radians range, is used for beam steering.

One of the basic functions of control devices in a phased-array antenna is to provide a planephase wavefront which propagates at an angle θ to the antenna surface. In its simplest form, this could be done by the insertion of a phaseshift in the feed to each element in the array so as to equalize the total phaseshift between the signal source and the desired phasefront. This is shown in Figure 1 for the extreme elements (0 and n) in a linear array. In present narrowband phased-array antennas, the absolute phaseshift is not equalized but rather phaseshifters, variable over a 0-2π range, are adjusted to produce a planephase front. This small phase variation can be used to steer even large arrays since contributions from individual elements will add in phase as long as their absolute phase differs only by 2nπ, where n is an integer. Use of 0-2π phaseshifters, however, limits the instantaneous bandwidth of the array.

For operation of phased array over a wide instantaneous frequency band, not only must the phase at each element be set to give the required beam angle at a certain frequency, say midband (ω_o), but the rate of change of phase with frequency must be set so as to keep the beam angle constant with variations in frequency. These conditions on the required phaseshift can be summarized as

Dwg. 7754A01

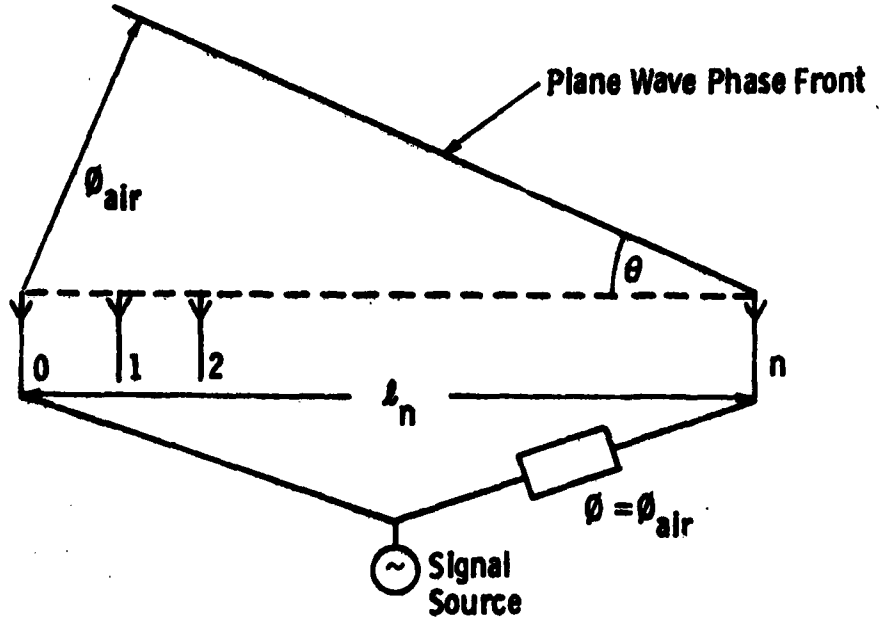

Figure 1 — Planephase front produced by array antenna.

$$\phi_n = \frac{\omega_o \ell_n}{V} \sin \theta \qquad [1]$$

and

$$\frac{\partial \phi_n}{\partial \omega} = \frac{\ell_n}{V} \sin \theta \qquad [2]$$

where ϕ_n is the phaseshift at element n, ω is the angular frequency, ℓ_n is the distance of the element from one end of the linear array, V is the velocity of light in air, and θ is the beam-pointing angle.

Obviously, the conditions given in Equations 1 and 2 are satisfied simultaneously by a nondispersive delay line, i.e., a delay line in which the phase velocity and group velocity are equal and invariant with frequency. However, magnetostatic wave delay lines are dispersive, as are lumped-constant, stripline, and folded-tape-meander delay lines. Here, dispersive means that the phase velocities and group velocities are not equal, and in the context of Equations 1 and 2,

$$\frac{\phi_n}{\omega} \neq \frac{\partial \phi_n}{\partial \omega} .$$

This implies that if the absolute phase at midband is set using a dispersive delay line to produce a beam angle θ, then any change in frequency will result in a change in θ. Thus, it appears that variable delay lines with dispersive characteristics cannot be used as the only phase-setting devices in an array. However, it will be possible to use a variable dispersive delay line, e.g., a magnetostatic wave device and a $0-2\pi$ phaseshifter as shown in Figure 2. Here, the phaseshifter sets the beam angle at midband and the delay line is adjusted so that

$$\frac{\partial \phi_n}{\partial \omega} = \frac{\ell_n}{V} \sin \theta .$$

The necessary phaseshift could be integrated with the GaAs power amplifier in an active aperture array. If, however, the delay lines are used to feed subarrays, as shown in Figure 3, then the dispersive nature of the magnetostatic wave delay line does not introduce an increase in component count.

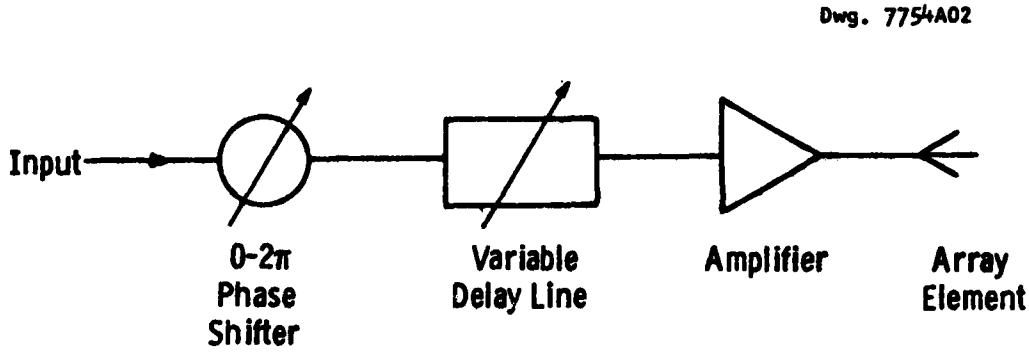

Figure 2 -- Phase control for antenna element using an MSW variable delay line plus a phaseshifter.

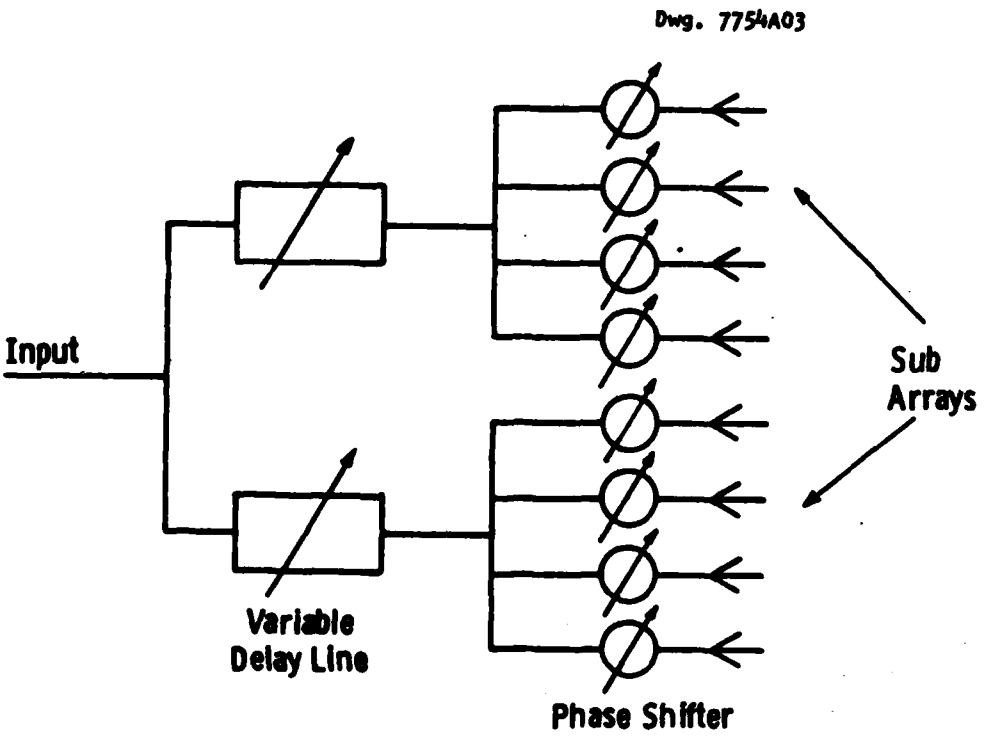

Figure 3 — Phase control using an MSW variable delay line in an antenna with subarrays.

2.2 A Constant-But-Adjustable Magnetostatic Delay Line

This section describes the design and construction of a constant-but-adjustable delay line using two "chirp" filters in series. This approach has been reported in the literature[1] using a surface wave (SW) "up-chirp" and a BVW "down-chirp" filter. It was decided in this work to use an FVW "up-chirp" filter instead of the SW filter and obtain improved bandwidth as a result. Figure 4 shows the basic idea of adding two "chirped" filter responses, then sliding one of the filter responses along the frequency axis to obtain an adjustable delay. This sliding was readily achieved by winding bias coils on the yoke of the permanent magnet assembly for the FVW delay line (see Figure 5). A dc current through these coils could shift the net bias field on the YIG film either up or down about the fixed value of 2.5 kG provided by the Sm-Co permanent-magnet polepieces and yoke assembly.

The delay calculations were performed for single 54-micron-thick YIG films grown epitaxially on GGG. Delay linearity was optimized by placing a single ground plane 54 microns from the YIG film for the FVW device and 400 microns for the BVW device. In Figure 4 the range of delay delineated by the arrows was the most linear region, and thus the delay lines were designed to work over this range. The two slopes were respectively calculated as 93 nS/GHz/cm and -68 nS/GHz/cm and, in order to equalize them numerically, the FVW delay line was designed to have a pathlength of 7.33 cm and the BVW delay line a 10-cm pathlength. The 54-micron spacing was achieved by grinding down a piece of Corning 7059 glass optically cemented to a gold-plated commercial alumina substrate. The 54-micron glass spacer then formed a dielectric spacer on which the microstrip feeds, and transducers were fabricated using conventional photolithography. For the 400-micron spacer, a conventional 25-mil alumina substrate was thinned down to 16 mils by grinding, and then microstrip feeds and transducers were defined photolithographically in 5-micron gold film. The YIG samples were cut from a 2-inch diameter wafer and measured 25 mm by 5 mm. Each was bevelled to 1° at the ends as an aid to suppressing MSW reflections. The static bias fields were

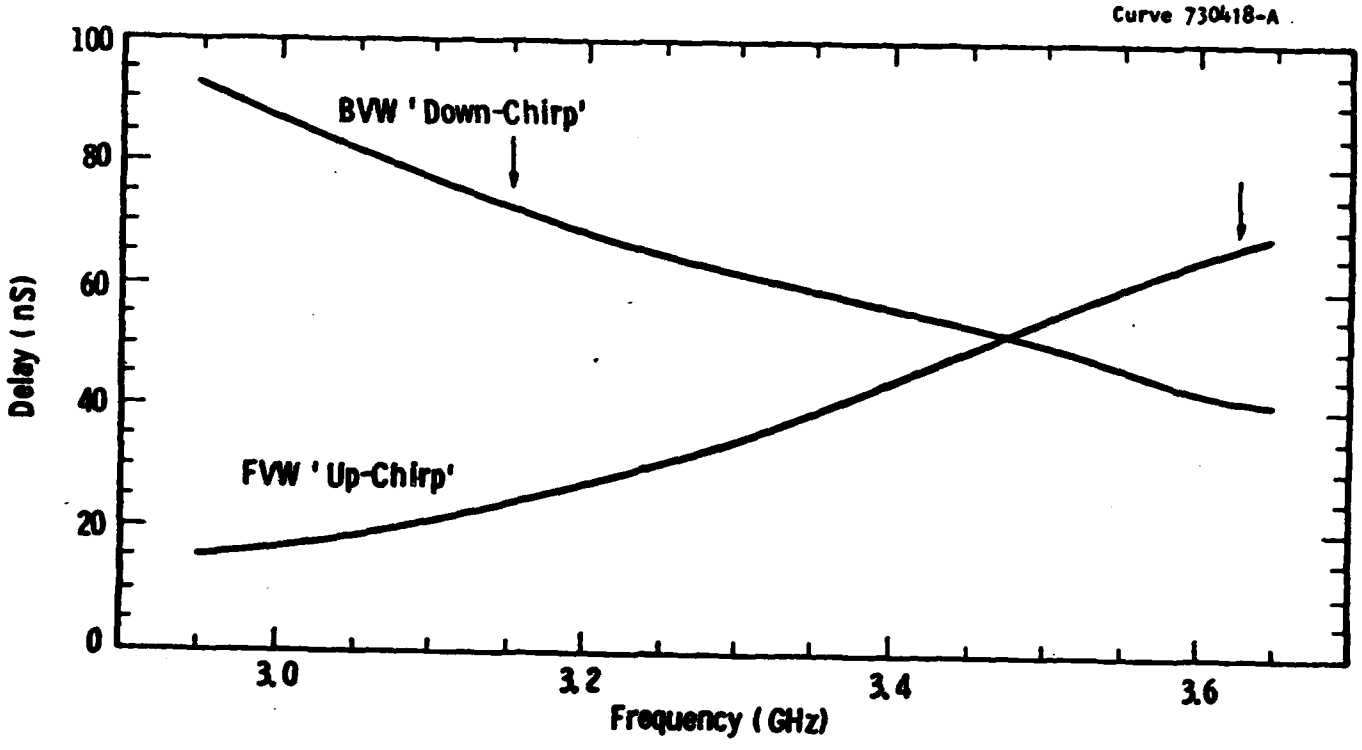

Figure 4 — Calculated delay versus frequency for two magnetostatic delay lines designed to give an optimum range of linear delay over the frequency range defined by the arrows: film thickness 54 microns, ground-plane spacing 54 microns (FVW) and 400 microns (BVW).

provided by Sm-Co polepieces. For the FVW delay line, a conventional type yoke machined from low-carbon steel surrounded these polepieces and gave a 3-mm airgap for the device. The typical field profile for this type of structure is shown in Figure 6. Over the active region of the YIG film, the field was uniform to about 0.1%. The BVW delay line was a more difficult design because the magnetic field must run parallel to the YIG film. The solution was to use only Sm-Co magnets with no yoke and magnetized on their small or end faces, as shown in Figure 7. Field calculations showed that for a given thickness of magnet there was optimum separation of the polepieces to give a maximum field uniformity over the YIG active region. In Figure 7 the 25-mm-square magnets gave a field uniformity of 1% over a 1-cm pathlength along the long axis of the YIG sample. Transverse to the long axis, the field uniformity was about 1.5% across the 5-mm width of the sample. Initial transmission measurements on both delay lines showed substantial interference from reflected triple-transit signals. The bevelled sample ends were not sufficient to suppress these. Additionally, the steep fall-off in magnetic field immediately beyond the transducers in the BVW device was certain to have caused reflections of the bidirectional waves. Fortunately, considerable improvement was achieved by evaporating a thin (~500Å) Al film on each end of the YIG films and extending up almost to where the transducers contacted the films. These Al films acted as areas of ohmic loss for the MSWs. The completed delay lines are shown in Figure 5. The bias coils on the FVW delay lines are clearly visible. These coils had a sufficient number of turns on them to cause a maximum 500-MHz shift in the operating frequency of the delay line when fed by a dc current of ≈1A.

The transmission loss (S_{21}) and delay versus frequency are shown for the BVW device in Figure 8. The transmission loss is quite smooth and ripple-free except in the vicinity of the bandedge at 3.55 GHz. The delay results reflect this performance. The 400-micron ground-plane spacing has ensured a fairly linear group delay from about 3.5 to 2.9

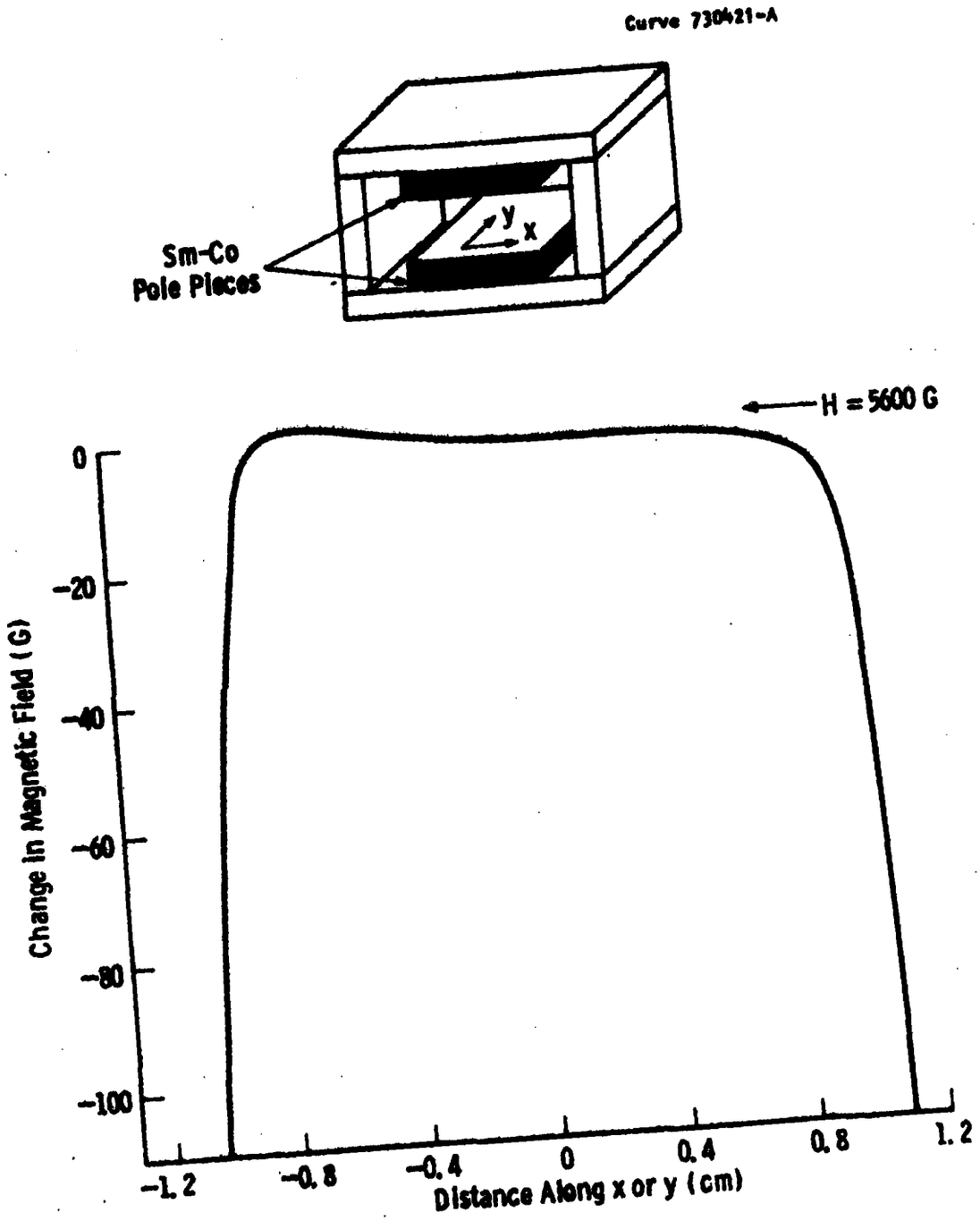

Figure 6 — Magnetic-field profile in the horizontal mid-plane of the 3-mm air gap for the FVW permanent magnet shown in the sketch.

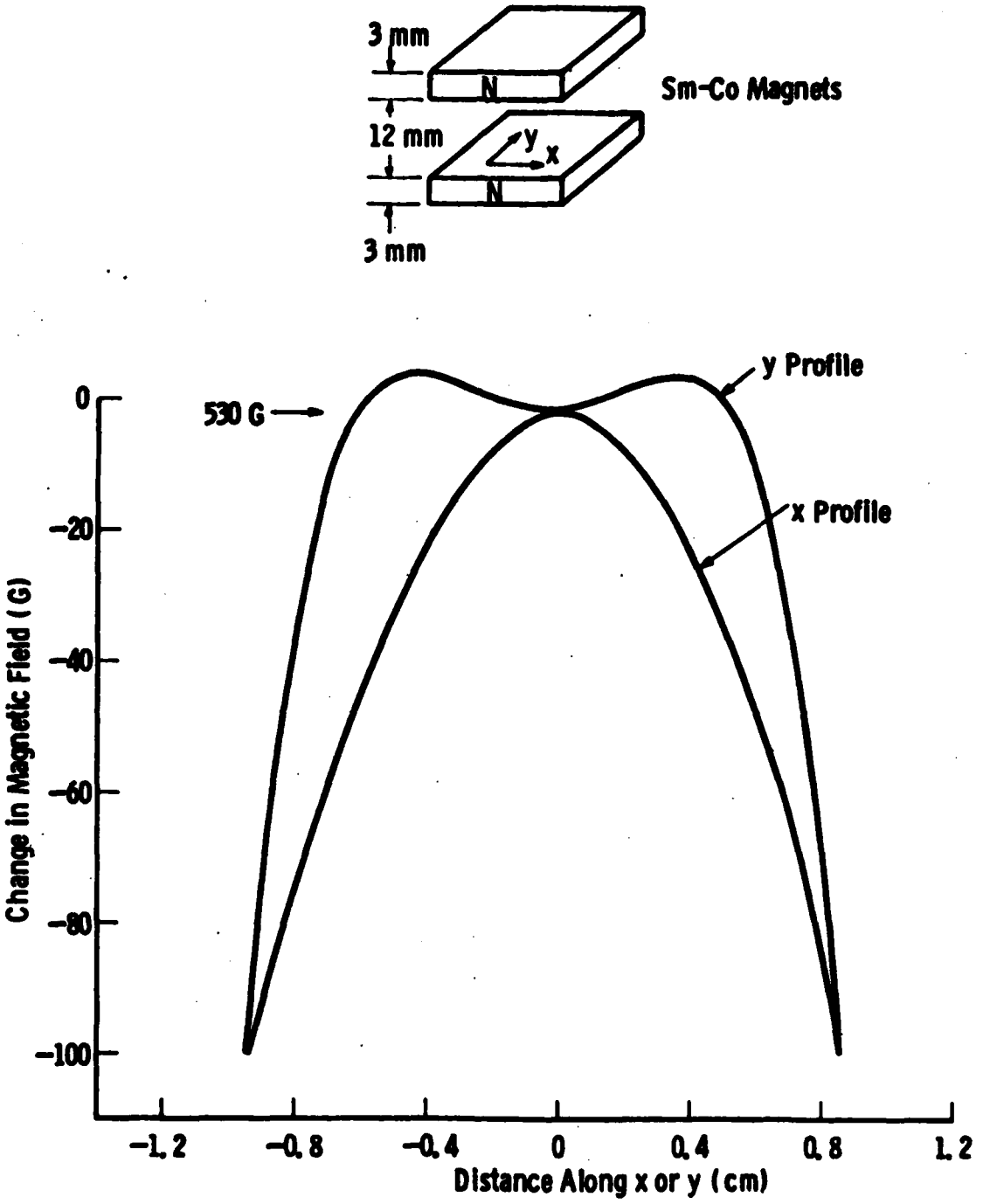

Figure 7 -- Magnetic-field profiles in the horizontal mid-plane of the 12-mm air gap for the BVW permanent magnet shown in the gap.

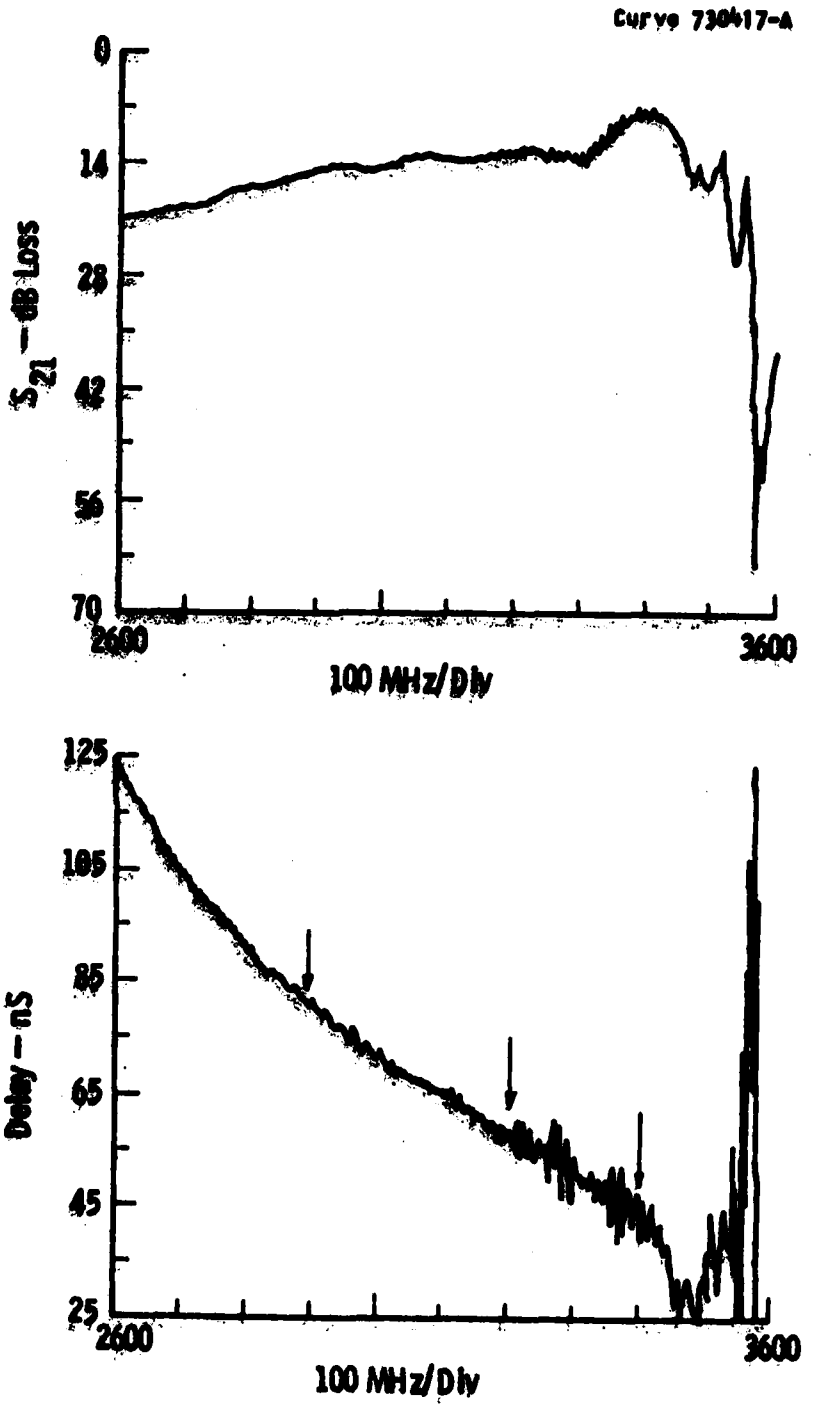

Figure 8 — Upper curve: transmission loss versus frequency for the BVW delay line over part of its bandwidth. Lower curve: delay versus frequency for the same delay line.

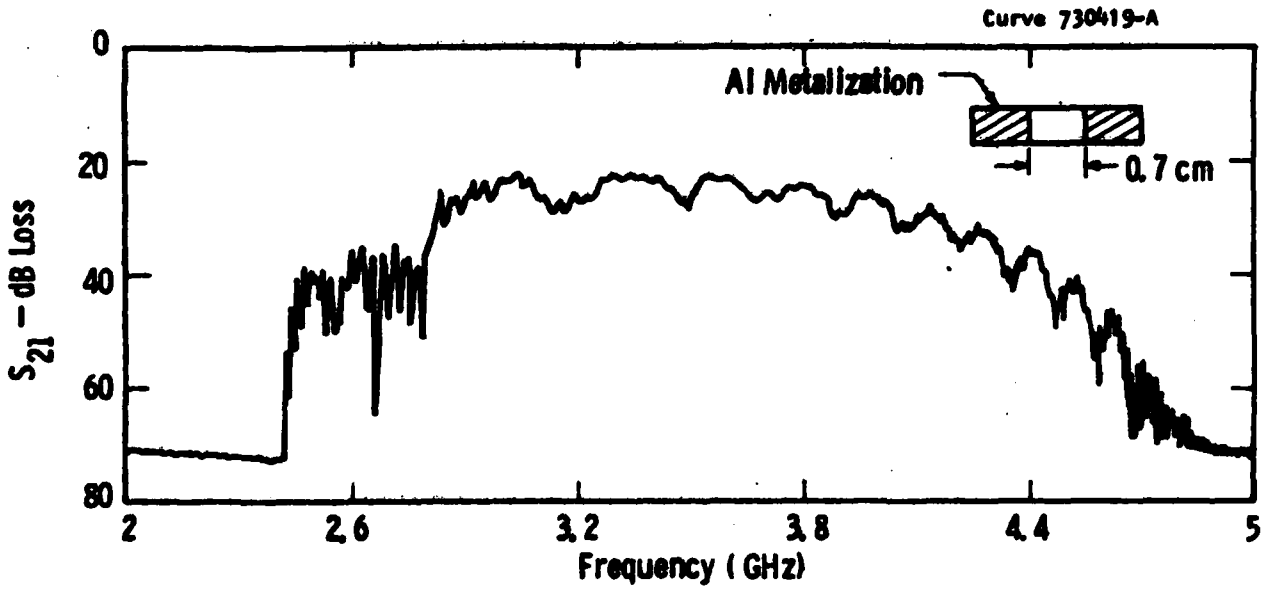

Figure 9 — Transmission loss versus frequency for the FVW delay line showing the undesirable effects of higher-order widthmode generation.

3. PROPAGATION AT AN ARBITRARY ANGLE TO THE BIAS FIELD

In order to investigate the delay properties of MSW as a function of magnetic-field orientation, the dispersion relation must be derived as a function of field orientation. Once the dispersion relationship is known, the phase and group velocities can be found. The task of generating these mathematical relationships for a ferrite film in close proximity to a ground plane is underway. Also underway is the design and fabrication of an MSW induction probe[5] that will be used to detect the waves for different walk-off angles as the direction of the magnetic field is varied. We will then be able to check theory against experiment.

So far the dispersion relationship has been derived for a ferrite film plus a ground plane where the z axis is taken to be normal to the film. The magnetic potential function used for the calculations in the film has the form

$$\psi(xyz) \propto e^{-jk_x x} e^{-jk_y y} e^{-jk_z z}. \qquad [3]$$

Inside the film, using the magnetostatic approximation, we have

$$\vec{\nabla} \cdot \vec{B} = 0$$

$$\vec{H} = \nabla\psi \qquad [4]$$

$$\vec{B} = \mu_o[\mu] \cdot \vec{H}$$

where $[\mu]$ is the permeability tensor for the internal field at an arbitrary angle. From Equation 4, the potential is found to satisfy the following equation in the magnetic medium.

$$\mu_{11}\frac{\partial^2\psi}{\partial x^2} + \mu_{22}\frac{\partial^2\psi}{\partial y^2} + \mu_{33}\frac{\partial^2\psi}{\partial z^2} + (\mu_{12} + \mu_{12}^*)\frac{\partial^2\psi}{\partial x\partial y} + (\mu_{13} + \mu_{13}^*)\frac{\partial^2\psi}{\partial x\partial z} + (\mu_{23} + \mu_{23}^*)\frac{\partial^2\psi}{\partial y\partial z} = 0 \qquad [5]$$

Using Equations 3 and 5 and solving for k_z, we obtain

$$k_{z1} = a+b$$

and

$$k_{z2} = a-b$$

where

$$a = \frac{-[(\mu_{13} + \mu_{13}^*)\, k_x + (\mu_{23} + \mu_{23}^*)\, k_y]}{2\mu_{33}}$$

and

$$b = \left\{\frac{[(\mu_{13} + \mu_{13}^*)\, k_x + (\mu_{23} + \mu_{23}^*)\, k_y]^2}{4\mu_{33}^2} - \frac{[\mu_{11} k_x^2 + \mu_{22} k_y^2 + (\mu_{12} + \mu_{12}^*) k_x k_y]}{\mu_{33}}\right\}^{1/2}.$$

Unequal wavenumbers k_z commonly arise because spin waves of a given frequency travel at a fixed angle to the magnetic field (exchange effects being neglected). For an asymmetric film orientation, therefore, the allowed spin-wave directions make unequal angles with the film. It follows that to achieve a given $k_{x,y}$ along the film, different k_z wavenumbers must be used. Therefore, the proper potential function is

$$\psi(xyz) = e^{-jk_x x}\, e^{-jk_y y}\, (Ae^{-jk_{z1} z} + Be^{-jk_{z2} z}). \qquad [6]$$

To get the dispersion relationship, we use the surface-permeability approach of Entage,[4] where the general form of the secular equation is

$$\mu^{sp} - \mu^{sn} = 0.$$

Taking the film to occupy the region from 0 to d along the z axis and to be infinite in extent in the x and y directions, the relative permeabilities are defined as

$$\mu^{sp} = \lim_{z \to +0} \frac{-i\ Bz}{\mu o H_T}$$

$$\mu^{sn} = \lim_{z \to -0} \frac{-i\ Bz}{\mu o H_T}$$

where $H_T = (H_x^2 + H_z^2)^{1/2}$ and Equation 4 is used to evaluate the magnetic field.

For a ground plane located at z = -t, the following dispersion relationship has been derived.

$$\tan bd = \frac{C\ k_T\ (1 + \tanh k_T t)}{A - k_T^2 \tanh k_T t - B\ k_T\ (1 - \tanh k_T t)}$$

where $A = \sin^2\theta\ [K^2(k_x \sin\phi + k_y \cos\phi)^2 + \mu(\mu-1)(k_x \cos\phi + k_y \sin\phi)^2]$

$$-\mu k_T^2\ (\cos^2\theta + \mu \sin^2\theta)$$

$$B = -K \sin\theta\ (k_x \sin\theta + k_y \cos\phi)$$

$$C = [\mu(\mu-1) \sin^2\theta\ (k_x \cos\phi + k_y \sin\phi)^2 - \mu k_T^2\ (\cos^2\theta + \mu \sin^2\theta)]$$

$$b = C/(\cos^2\theta - \mu \sin^2\theta)$$

$$k_T = (k_x + k_y)^{1/2}$$

$$\mu = 1 + \frac{\Omega_H}{\Omega_H^2 - \Omega^2} \quad ; \quad K = \frac{\Omega}{\Omega_H^2 - \Omega^2}$$

and the angle θ is measured from the z axis to H_{int} and the angle ϕ is measured from the x axis to the projection H_{int} onto the x,y plane.

We have not programmed the expression yet, therefore we have no plots of wavenumber versus frequency to show at this time.

4. MAGNETOSTATIC WAVE PROPAGATION IN DOUBLE FILMS

The problem of linearizing the group delay over some useful range of bandwidth for FVWs and BVWs had previously been addressed through the use of a close proximity ground plane.[2] Although a ground plane could modify the dispersive behavior of magnetostatic waves to give a quasilinear delay characteristic, a penalty was paid in terms of increased insertion loss due to ohmic losses in the plane.[2] This prompted an interest to investigate the magnetostatic modes of propagation in two films coupled by their close proximity. Although in the analysis ground planes were included for completeness, it was hoped that useful delay versus frequency behavior would result with their influence much reduced, i.e., spaced far away from the magnetic films. It was realized at the time this work was started that the analytical approach to the dispersion relation would lend itself very well to applying the concept of "surface permeabilities."[4] This indeed proved to be the case and the double-film analysis and results to date are fully reported in Appendices I and II.

In summary, double films were found to support both FVWs and BVWs. Depending on the magnetic-film parameters, geometry, and mode symmetry, these waves could exhibit either constant delays or linearly varying delays over bandwidths of up to 0.4 GHz and 1 GHz, respectively. This was achieved with a negligible influence from ground planes. Preliminary measurements on separate YIG films sandwiching transducers were performed which confirmed the essential correctness of the analysis. Measurements on double YIG films grown compositely are presently in progress.

5. EPITAXIAL GROWTH OF GGG FILMS

GGG film growth by lpe was investigated as a possible nonmagnetic, dielectric spacer medium between two YIG films. Initial epitaxial growth was performed using one-inch diameter GGG substrates and the first of the melt compositions listed in Table 1. Melt 1 is approximately the same as that reported previously[6] as a polish for GGG. Films were grown from melt 1, but it was not possible to supersaturate the melt by more than a few °C without the formation of crystallites which floated on the melt surface and caused defects in the epitaxial film. The composition of the crystallites was not determined, but a comparison of the Ga_2O_3/Gd_2O_3 molar ratio (2) with the Fe_2O_3/Y_2O_3 ratio (>12) in a YIG melt indicated that the crystallites may possibly be a second phase. Because of this, the amount of Ga_2O_3 in the melt was doubled in composition 2 of Table I. It was possible to supersaturate melt 2 by 10°C or more without crystallite formation. Unfortunately, the saturation temperature was 1065°C, which is higher than desirable for lpe owing to rapid PbO evaporation. In melts 3 and 4, the PbO/B_2O_3 ratio was kept constant but the $(PbO + B_2O_3)/(Gd_2O_3 + Ga_2O_3)$ ratio was increased. This decreased the saturation temperature to below 950°C as desired. The dependence of growth rate on melt temperature is shown in Figure 10 for compositions 1 to 6.

X-ray measurements showed a lattice mismatch of approximately 0.006Å for films of melts 1 through 4. This was anticipated since the Czochralski-grown GGG substrate material is nonstoichiometric and has a lattice parameter of 12.382Å compared with the stoichiometric value of 12.376Å. An epitaxial GGG layer 39 μm thick was grown on a 20-μm thick epitaxial YIG film which had been grown on a GGG substrate. The GGG and YIG films were cracked on cooling to room temperature after growth.

TABLE I. MELT COMPOSITIONS FOR GGG EPITIAXIAL GROWTH

Melt Composition	Weight in grams					Saturation temp. °C	Film/Substrate lattice Mismatch Å
	PbO	B_2O_3	Ga_2O_3	Gd_2O_3	Sm_2O_3		
1	2753.1	73.5	87.9	85.5	—	946	
2	2753.1	73.5	175.82	85.5	—	1065	~.006
3	3207.1	85.6	175.82	85.5	—	998	
4	3000.0	80.5	128.18	62.33	—	950	
5	3165.0	84.91	135.23	62.33	3.32	946	~.004
6	3330.0	89.32	142.28	62.33	6.63	941	~.002

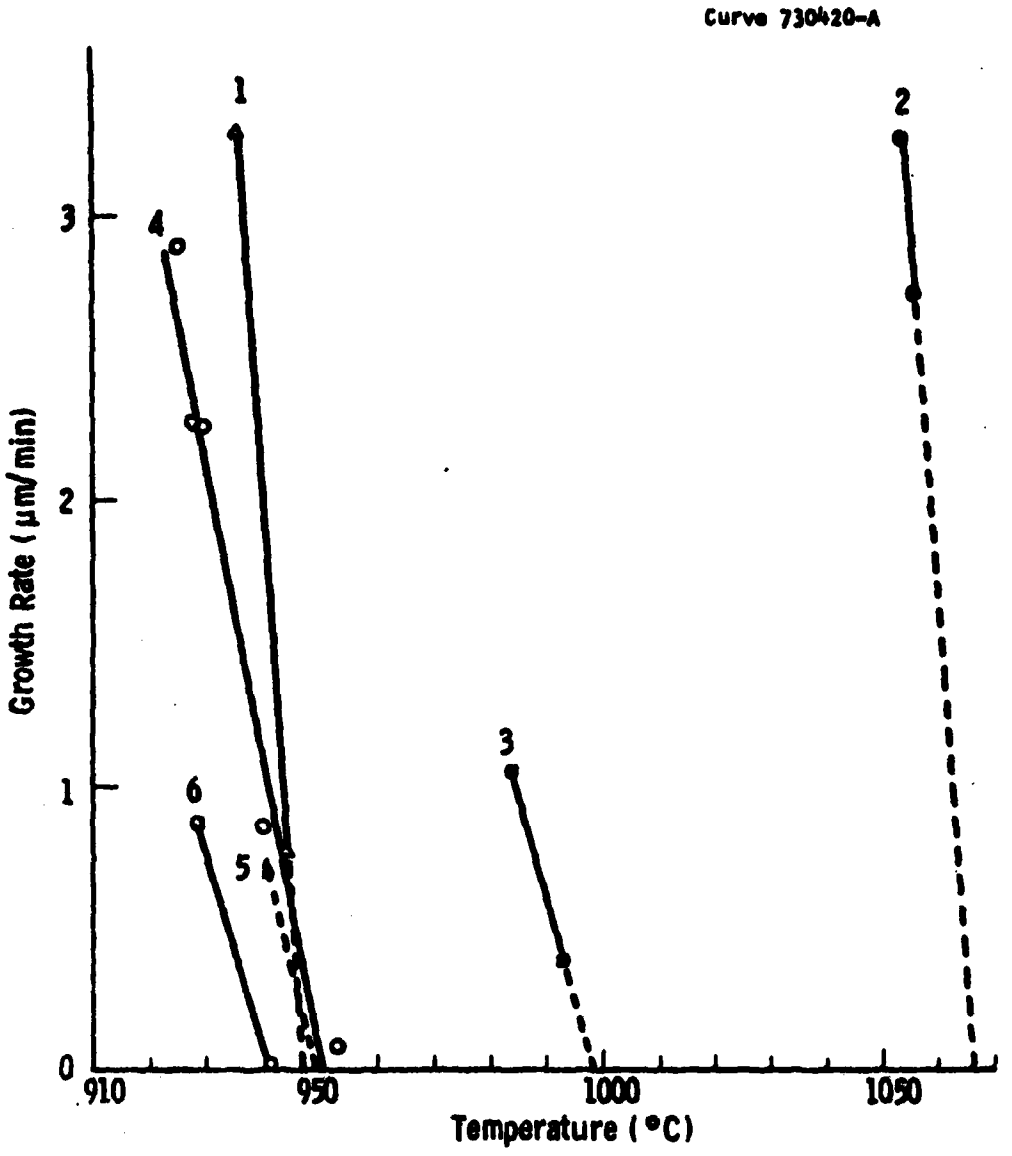

Figure 10 — Growth rate as a function of temperature for melt compositions listed in Table I.

6. CONCLUSIONS AND FUTURE WORK

Magnetostatic wave delay lines will require the use of phaseshifters to set the appropriate midband beam angle when they are used in phased arrays. This should not present difficulties in active-aperture arrays, especially if subarrays are used. The combined BVW and FVW variable delay line has been demonstrated to yield variable delay. However, the FVW device requires more work to remove amplitude ripples. This type of structure may meet phase-error ($<5^{o}$) requirements of small-aperture antennas even with the use of simple, single YIG-film structures. Large apertures, however, require longer delay times so that the phase errors in MSW delay lines become more significant and must be minimized. Dispersion relations for propagation at an arbitrary angle have been derived but have not been programmed at present. Further work on this topic together with experimental measurements are planned for the near future.

The theory for FVW and BVW propagation in a double YIG film has been developed and initial experiments have demonstrated that this is a promising technique. Work on transducers for MSW in double YIG films shows that special structures may be required to launch the MSW into the required odd or even mode. Once the composition of the Sm:GGG melt is optimized to yield films with a close lattice-match Czochralski-grown GGG, then the growth of epitaxial YIG/GGG/YIG structures will be performed. The main thrust during the remainder of this program will be to develop techniques which reduce the phase error and amplitude ripple of both "up-chirp" and "down-chirp" delay lines. In addition, other techniques to achieve variable delay, such as multitapped delay lines, will be investigated.

7. REFERENCES

1. J. C. Sethares, J. M. Owens, and C. V. Smith, Jr., "MSW Nondispersive, Electronically Tunable Time Delay Elements," Electronics Letters, 16:825 (1980).

2. J. D. Adam, Michael R. Daniel, T. W. O'Keeffe, and P. R. Emtage, "Magnetic Surface Wave Device Technology," Final Report, Contract No. F33615-77-C-1068, USAF Wright Patterson AFB (Aeronautical Systems Division).

3. Michael R. Daniel, J. D. Adam and T. W. O'Keeffe, "Linearly Dispersive Delay Lines at Microwave Frequencies Using Magnetostatic Waves," IEEE Sonics and Ultrasonics Conference, New Orleans (1979), IEEE Cat. No. 79CH1482-9.

4. P. R. Emtage, "Interaction of Magnetostatic Waves with a Current," J. Appl. Phys., 49: 4475 (1978).

5. C. V. Smith, Jr. J. M. Owens, T. J. Mears II, and N. D. Parkih, "Induction Probing of Magnetostatic Delay Line Fields," IEEE Trans, MAG-15:1738 (1979).

6. J. M. Robertson, M. J. G. van Hout, M. M. Jansen, and W. T. Stacy, "Garnet Substrate Preparation By Homoepitaxy," J. Cryst. Growth, 18:194 (1973).

EFFORT EXPENDITURE

The contractual hour requirements are:

3800 professional hours
1260 technical hours

Cumulative Hours expended up to 30 September 1981:

1834 professional hours
560 technical support hours

Percent technical completion 47%
Projections for effort expenditure are being met.

APPENDIX A

MAGNETOSTATIC VOLUME WAVE PROPAGATION IN A FERRIMAGNETIC DOUBLE LAYER*

Michael R. Daniel and P. R. Emtage
Westinghouse Research & Development Center
Pittsburgh, PA 15235

ABSTRACT

Using the technique of "surface permeabilities," an expression is derived for the dispersion of magnetostatic waves propagating in two close proximity ferrimagnetic films. Two modes of propagation for volume waves are identified respectively as the symmetric and antisymmetric modes from the symmetry of the rf magnetization. Useful group delay behavior is shown to result from films of equal thickness. Some measurements are reported using two yttrium iron garnet films sandwiching simple single finger transducers. Difficulties in exciting the symmetric forward volume mode are explained in terms of the coupling coefficients for these double film structures.

I. INTRODUCTION

There have recently been a number of papers,[1]-[3] of a mostly theoretical nature, describing the propagation of magnetostatic surface waves in two ferrimagnetic films coupled together by their close proximity. Scant attention has been given to the propagation of magnetostatic volume waves in a double film structure. Our interest in the volume waves was motivated by practical considerations to see if they offered any useful time delay characteristics for microwave delay-line applications. Additionally, the problem provided an opportunity to demonstrate the useful technique of "surface permeabilities"[4] in a relatively complicated situation. We will describe the propagation characteristics for forward volume waves (FVWs) in which the static magnetic bias field is applied normal to the plane of the films, and also for backward volume waves (BVWs) with the bias field in-plane and parallel to the propagation direction. Measurements of time delay versus frequency are presented for epitaxially grown Yttrium Iron Garnet (YIG) films. Finally, transducer coupling strengths are calculated for films of equal thickness; these coupling strengths help to explain some of the experimental results.

II. THEORY

A. Introduction

i. General. The surface permeability μ^s is useful in the analysis of systems with plane parallel discontinuities (such as magnetic films) because its value at each interface can be calculated from its value at the interface above or below[4],[5] (see Equation 7); further, μ^s is known at the upper and lower boundaries of the system, which are metal or vacuum. For a sample of N layers, therefore, N algebraic iterations yield the secular equation; this process is simpler than the usual method of solving 2N simultaneous equations for the field amplitudes.

We consider waves travelling along the x-axis in a film bounded by planes y = const. The field $\underline{h}$ and flux density $\underline{b}$ are

$$b_x/\mu_o = \mu_{11}\, h_x + i\, \mu_{12}\, h_y,$$

$$b_y/\mu_o = -i\, \mu_{12}\, h_x + \mu_{22}\, h_y. \qquad (1)$$

In the magnetostatic approximation we set $\underline{h} = \underline{\nabla}\psi$, where ψ is a potential. From $\underline{\nabla}.\underline{b} = 0$, Eq. (1) yields

$$\mu_{11} \frac{\partial^2 \psi}{\partial x^2} + \mu_{22} \frac{\partial^2 \psi}{\partial y^2} = 0 . \qquad (2)$$

A magnetostatic wave of wave number k along the x axis is therefore derived from a potential

$$\psi = e^{i(kx - \omega t)} \left[Ce^{\beta k y} + De^{-\beta k y}\right], \qquad (3)$$

where

$$\beta^2 = \mu_{11}/\mu_{22}, \tag{4}$$

and where C and D are constants found from the boundary conditions.

ii. The Surface Permeability. The surface boundary conditions are that the tangential field, h_x, and the normal flux, b_y, be continuous across an interface y = const. These conditions are satisfied if the ratio b_y/h_x, which has the dimensions of a permeability, is continuous everywhere.

We therefore define a relative surface permeability μ^s as

$$\mu^s(y) = -ib_y(y)/\mu_o h_x(y), \tag{5}$$

where the factor i is introduced because b_y and h_x are out phase.

Consider a magnetic system extending between y_{min} and y_{max}. The magnetic potential ψ in Eq. (3) must be small far from the system. For positive k, then, the constants in Eq. (3) are C = 0 when $y > y_{max}$, and D = 0 when $y < y_{min}$. In the vacuum regions, therefore,

$$\mu^s = \pm 1, \ (y > y_{max}), \tag{6a}$$

$$\mu^s = \mp 1, \ (y < y_{min}),$$

the upper or lower signs being taken as k is positive or negative. If one of the limits of the system is a perfectly conducting metal layer, where $b_y = 0$, then the boundary condition becomes

$$\mu^s = 0, \text{ (metal layer)}. \tag{6b}$$

Suppose that μ^s is known in the plane $y = y_1$ and that a continuous medium extends between y_1 and y_2. The ratio C/D in Eq. (3) can be found from $\mu^s(y_1)$, and $\mu^s(y_2)$ can then be calculated. The result is

$$\mu^s(y_2) = \frac{\mu_{22}\mu^s(y_1) + [\mu_{11}\mu_{22} - \mu_{12}^2 - \mu^s(y_1)\,\mu_{12}]\,\beta^{-1}\tanh \beta k\,(y_1 - y_2)}{\mu_{22} + [\mu^s(y_1) + \mu_{12}]\,\beta^{-1}\tanh \beta k\,(y_1 - y_2)} \quad (7)$$

Therefore we can use Eq. (7) to iterate μ^s from an upper (or lower) surface where it is known, through Eqs. (6), until we reach another surface where it is known. The secular equation is obtained by requiring that these values be the same.

More generally, in a system of N layers there are discontinuities at $y_1, y_2, \cdots y_{N+1}$ ($y_1 > y_2$, etc.); $\mu^s(y_1)$ and $\mu^s(y_{N+1})$ are known from the boundary conditions. Denote by $\mu^{sp}(y_i)$ the value of μ^s at y_i calculated from all layers above y_i, and by $\mu^{sn}(y_i)$ the value found from all layers below y_i. Thus

$$\begin{aligned} &\mu^s(y_1) \to \mu^{sp}(y_2) \cdots \to \mu^{sp}(y_i), \\ &\mu^s(y_{N+1}) \to \mu^{sn}(y_N) \cdots \to \mu^{sn}(y_i), \end{aligned} \quad (8)$$

where the sign $\to$ means 'leads to'. The secular equation is

$$\mu^{sp}(y_i) = \mu^{sn}(y_i). \quad (9)$$

The use of this procedure is demonstrated below.

B. Secular Equations

i. Single Layer. For a magnetic layer extending between y = 0 and y = d we have μ^s (d) = $\pm$ 1, μ^s (0) = $\mp$ 1. Equations (7) and (9) then give

$$\frac{1}{\beta} \tanh \beta kd = \frac{\mp 2\mu_{22}}{\mu_{11}\,\mu_{22} + 1 - \mu_{12}^2}, \qquad (10)$$

which is the usual result for a single layer.

ii. Double Layer. We consider the system sketched in Fig. 1. Upper and lower layers of thicknesses d_1 and d_2 are separated by a vacuum layer extending between y = 0 and y = t. There are ground planes at distances s_1 above the upper layer and s_2 below the lower layer.

The surface permeabilities at the ground planes are μ^s = 0, from Eq. (6b). At the upper and lower magnetic surfaces, therefore, Eq. (7) gives

$$\mu^{sp}\,(t + d_1) = \tanh ks_1,$$

$$\mu^{sn}\,(-d_2) = -\tanh ks_2.$$

These ratios tend to $\pm$ 1 when s is large, as Eq. (6a) requires. From Eq. (7), the surface permeabilities at the edges of the central vacuum layer are

$$\mu^{sp}(t) = \frac{\mu_{22}^{(1)} \tanh ks_1 + [\mu_{11}^{(1)}\mu_{22}^{(1)} - (\mu_{12}^{(1)})^2 - \mu_{12}^{(1)} \tanh ks_1]\,\beta_1^{-1} \tanh \beta_1 kd_1}{\mu_{22}^{(1)} + [\tanh ks_1 + \mu_{12}^{(1)}]\beta_1^{-1} \tanh \beta_1 kd_1}, \qquad (11)$$

$$\mu^{sn}(0) = -\frac{\mu_{22}^{(2)} \tanh ks_2 + [\mu_{11}^{(2)}\mu_{22}^{(2)} - (\mu_{12}^{(2)})^2 + \mu_{12}^{(2)} \tanh ks_2]\,\beta_2^{-1} \tanh \beta_2 kd_2}{\mu_{22}^{(2)} + [\tanh ks_2 - \mu_{12}^{(2)}]\beta_2^{-1} \tanh \beta_2 kd_2}.$$

These quantities each involve the properties of one layer only. The secular equations for waves of positive or negative k on either layer alone (together with the associated ground plane) are

$$D^{(1)}_{\pm} \equiv \mu^{sp}(t) \pm 1 = 0 \qquad , \quad D^{(2)}_{\pm} \equiv \mu^{sn}(0) \mp 1 = 0 \cdot \tag{12}$$

The interaction of the films through the vacuum layer between 0 and t is obtained by calculating $\mu^{sp}(0)$ from $\mu^{sp}(t)$; Eq. (7) gives

$$\mu^{sp}(0) = \frac{\mu^{sp}(t) + (1 - \mu^{sp}(t)) \tanh kt}{1 + \mu^{sp}(t) \tanh kt}. \tag{13}$$

On equating this to $\mu^{sn}(0)$, we obtain the secular equation

$$D^{(1)}_{+} D^{(2)}_{+} - D^{(1)}_{-} D^{(2)}_{-} e^{-2kt} = 0, \tag{14}$$

where the D's are defined in Eq. (12). When kt is large and positive, the second term represents a weak interaction between modes that belong predominantly to each film separately.

iii. Symmetric System. When the two interacting layers are of the same material and thickness, with equidistant ground planes, it is still not the case that $D^{(1)} = \pm D^{(2)}$ unless $\mu_{12} = 0$. This inequality is associated with the fact that $D^{(1)}$ is constructed from μ^{sp}, while $D^{(2)}$ is constructed from μ^{sn}. It is therefore impossible to obtain symmetric or antisymmetric modes except in the case of volume waves ($\mu_{12} = 0$).

In a symmetric system with $\mu_{12} = 0$, Eqs. (11) yield $\mu^{sp}(t) = -\mu^{sn}(0)$; from Eq. (14), we find

$$\mu^{sn}(0) = \tanh \tfrac{1}{2} kt, \text{ (even in } \psi), \qquad \coth \tfrac{1}{2} kt, \text{ (odd in } \psi). \tag{15}$$

These modes are identified as even or odd in the magnetostatic potential because, in the central vacuum region, they correspond to $\psi \sim \cosh k\,(y - \frac{1}{2}t)$, $\sinh k\,(y - \frac{1}{2}t)$ respectively (the plane $y = \frac{1}{2}t$ is the center of the system).

Volume waves exist only in the region $\mu_{11}\mu_{22} < 0$. The quantity β in Eq. (4) is then imaginary, and we define

$$\alpha^2 = -\beta^2 = -\mu_{11}/\mu_{22}. \tag{16}$$

The secular equation is now

$$\tan \alpha\, kd = \frac{\mu_{22}\,\alpha\,(\tanh ks + \mu^{sn}(0))}{\mu_{22}^2\,\alpha^2 - \mu^{sn}(0)\tanh ks}, \tag{17}$$

where $\mu^{sn}(0)$ is given in Eq. (15).

In the following discussion we shall always refer to the fundamental mode as symmetric, even though, for backward volume waves, that mode is odd in the magnetostatic potential. For these waves the applied magnetic field is along the x-axis, so the excursion in the magnetization is in the y-direction. An odd magnetostatic potential therefore gives rise to a symmetric excitation of the system, and we regard the excitation as more significant than the potential.

This is illustrated in Fig. 2, which shows the rf field parameters $m_x(y)$ and $h_x(y)$ for FVWs and $m_y(y)$ and $h_x(y)$ for BVWs. The particular examples chosen were for two films of equal thickness 20 microns, spaced 40 microns apart. The ordinate values in Fig. 2 were derived from a magnetostatic potential function normalized to unity on the lower face of film #2. The static bias field (H) and frequency (f) were chosen to yield approximately equal wavevector (k) values for the symmetric FVW and BVW modes. It will be noted that the symmetric mode, as judged from the symmetry of the magnetization, is in both cases the fundamental mode, as judged from the wavenumber.

III. RESULTS

A. Calculations

The subsequent results were obtained from numerical solutions of Equation 17 (for dissimilar films Equation 14 is solved). Unless noted otherwise the following parameters were used: $S_1 = S_2 = 1$ cm; $4\pi M_1 = 4\pi M_2 = 1.8$ kG; $H_{FVW} = 3.214$ kG and $H_{BVW} = 2.991$ kG. This equation yields two sets of roots which have been termed the symmetric (S) and antisymmetric (A) modes. Each set corresponds to a fundamental thickness mode and an infinite sequence of higher order modes. The group delay data are the derivatives $(\frac{1}{2\pi} \frac{dk}{df})$ of the dispersion curves expressed in nS for a 1 cm path length. We recognized that Equation 14 or 17 can yield a substantial harvest of results from the permutation of all the parameters they contain. However, the following generalities did emerge: interesting results, i.e., results significantly different from those of FVW or BVW propagation in single films, are obtained from films of equal or nearly equal thickness; useful results in the context of yielding linear or constant group delays are obtained from films spaced 1 to 2 film thicknesses apart.

In Fig. 3 (upper) we illustrate the effects of different interaction strengths for the symmetric mode for FVWs in 20 micron thick films. When the film separation, t, is zero the dispersion curve is appropriate to a FVW in a single coalesced film of 40 microns thickness. When $t \to \infty$ the dispersion corresponds to a FVW in an isolated 20 micron film. The film separation has a significant effect on the group delay and we note parenthetically that a value of t = 30 micron gives a useful range of quasi-linear delay from approximately k = 100 to k = 1000 cm^{-1}.

Figure 4 shows the dispersion and group delay results for the fundamental S- and A-modes of FVWs and BVWs in two 20 micron thick films. From an applications point of view it was generally found that the S-mode has quasi linear group delay variation with frequency and the A-mode shows some region of quasi constant delay. The t values of 40 microns for the FVW and 30 microns for the BVW were in fact found to give optimum group delay linearity over bandwidths of about 1 GHz for the S-mode.

One feature peculiar to double films was found for those of different magnetizations. In an external bias field, H_o, these films have different operating bandwidths for magnetostatic wave excitation (γH to $\gamma\sqrt{H\ (H + 4\pi M)}$) due to different demagnetizing fields and different $4\pi M$ values. For overlapping, but not coincident, bandwidths the dispersion relations are discontinuous. This is illustrated in Fig. 5 for magnetizations of 1.8 and 1.4 kG respectively. If the internal bias field in film #1 is H then it is $(H + 4\pi M_1 - 4\pi M_2)$ in film #2 for the FVW geometry. In Fig. 5 (upper) between 9 and 10.12 GHz $\mu_{11}(1) < 0$ and $\mu_{11}(2) > 0$ for H = 3.214 kG. Film #1 supports most of the magnetostatic volume wave which decays exponentially in film #2. This is shown by the potential plots in Fig. 6. Both the S- and A-modes show this decay feature in film #2, however, the symmetry features are now gone and the terms symmetric and antisymmetric no longer describe the rf parameters. At 10.12 GH_z $\mu_{11}(2) \to \pm\infty$ and a discontinuity appears in the dispersion curves. Above 10.12 GHz both μ's are negative and "normal" propagation resumes, the dispersion curves re-start at k = 0. For BVW's with H in the plane of the films there is no change in the internal bias field H, but the upper frequency limit is down shifted in film #2 due to the lower $4\pi M_2$ value. In Fig. 5 (lower) above 10.15 GHz $\mu_{22}(1) < 0$ and $\mu_{22}(2) > 0$, the BVW is carried primarily in film #1 with an exponential decay in film #2. At 10.15 GH_z $\mu_{22}(2) = 0$ but the propagation constant β is singular since $\beta = \frac{1}{\sqrt{\mu_{22}}}$ and a discontinuity

in the dispersion curves result. Below 10.15 GHz both μ's are negative and "normal" propagation occurs.

B. Experiments

Three possible transducer configurations for exciting magnetostatic waves in a double film are shown in Fig. 7. The conductors supporting the microwave currents J could be either fine wires or conducting metal strips defined photolithographically. In the first experiment configuration (a) was used. Two 20 micron thick YIG films, grown epitaxially on gadolinium gallium garnet substrates, were cut into rectangular samples 3 mm by 25 mm. The transmitting and receiving transducers were 25 micron diameter gold wires which also acted as the spacers to keep the films 25 microns apart. Group delay measurements were performed on a network analyzer (HP model 8410B) under computer control (HP model 9845B). The static bias field was provided by a 12-inch Varian magnet. The results for FVWs are shown in Fig. 8 and for BVWs in Fig. 9. From the geometry of Fig. 7(a) the rf field h_x has odd symmetry in the films. Hence, by Fig. 2 the FVW should be an A-mode and the BVW an S-mode. Comparing the group delay results in Fig. 4 with the experimental results confirms this deduction. In fact, the experilental results were found to be in very good agreement with calculation. There was considerable interest in trying to excite the FVW S-mode due to its linear group delay behavior. Transducer configuration 7(b) was chosen for this. The transducers were made from gold ribbon 12 microns by 50 microns in cross section. These were driven by anti-phase currents from a microstrip power divider. The transducer pair elements and films were kept apart by several layers of a commercial polymer film (Saran wrap). The group delay results are shown in Fig. 10. The two noteworthy features of these results are the substantial noise or interference and the delay behavior more characteristic of an A-mode, see Fig. 8.

IV. CONCLUSIONS

Using a technique termed "surface permeabilities" a general expression was derived for the dispersion relation of magnetostatic waves propagating in two ferri-magnetic films coupled by their close proximity. From the symmetry of the rf magnetization within the films two sets of modes were identified for FVWs and BVWs termed the symmetric and anti-symmetric respectively. Additionally, two films of different static magnetization ($4\pi M$) were found to support a magnetostatic wave in a frequency range normally outside that for propagation in the lower value film. Group delay measurements were performed on epitaxially grown YIG double films which confirmed the dispersion analysis and mode identification. However, coupling constant calculations for the two modes showed that the relative excitation strength of each was transducer geometry dependent. In practice, it may prove difficult to always excite one desired mode without stimulating the second to some degree.

V. ACKNOWLEDGEMENTS

The authors would like to recognise Dr. J. D. Adam for his sustained interest and stimulating discussions regarding all aspects of magnetostatic waves. The continued technical assistance of J. Kerestes throughout the work is also gratefully acknowledged.

REFERENCES

*Work supported in part by U.S. Air Force (RADC) under contract number F19628-80-0150.

1. L. R. Adkins and H. L. Glass, Electronics Letters, 16, 503 (1980).
2. P. Grünberg, Journal of Applied Physics, 51, 4338, (1980).
3. Hiroshi Sasaki and Nobuo Mikoshiba, Journal of Applied Physics, 52, 3546 (1981).
4. P. R. Emtage, Journal of Applied Physics, 49, 4475, (1978).
5. This concept of surface permeability is similar to that of surface impedance used in electrical engineering problems.

Appendix: Coupling to a Current

We shall treat the generation of magnetostatic waves in the system sketched in Figure 7(b), where the stimulating currents J_1 and J_2 are between the two films. Results for exterior currents, as in Figure 7(c), are given at the end. The method is that of Reference 4, except that two sheets of current are present. The influence of the ground plane will be neglected.

Let $b_k(y)$ and $h_k(y)$ be the Fourier transforms of b_y and h_x in the plane y = const.

$$b_y(x,y) = \frac{1}{2\pi} \int b_k(y)\, e^{ikx}\, dk, \text{ etc.}$$

The current sheet J_1 in y = t gives rise to the field discontinuity

$$h_x(x,t+) - h_x(x,t-) = -j_1(x).$$

Upon taking Fourier transforms, using the definitions of μ^s, μ^{sn}, μ^{sp} in Equations (5) and (8), and noting that b_y is continuous across y = t, we obtain

$$b_k(t) = i\,\mu_o\, j_1(k)\, \mu^{sp}(t)\, \mu^{sn}(t)/[\mu^{sp}(t) - \mu^{sn}(t)], \qquad \text{(A1)}$$

where $j_1(k)$ is the Fourier transform of the current $j_1(x)$.

It is convenient to obtain the total field in the plane y = 0, where the second current sheet J_2 flows. The algebra is greatly simplified if we note that we shall later integrate b_k over k in order to obtain the field at large distances. The dominant contribution comes from the pole at $\mu^{sp} = \mu^{sn}$, and we can use this substitution everywhere except in the denominator. In the plane y = 0, the field $b_k^{(1)}$ due to J_1

is found to be

$$b_k^{(1)}(0) = irj_1 \mu_o (\mu^s(0))^2/[\mu^{sp}(0) - \mu^{sn}(0)], \tag{A2}$$

where

$$r = \cosh kt - \mu^s(0) \sinh kt. \tag{A3}$$

The total flux due to both currents is a similar quantity proportional to $j_2 + rj_1$. Upon taking Fourier transforms, the travelling field on the right of the transducer is found to be

$$b_y(x) = \mu_o(\mu^s(0))^2 (j_2 + rj_1) e^{ikx}/\frac{\partial}{\partial k} [\mu^{sp}(0) - \mu^{sn}(0)] \tag{A4}$$

where k is now the root of the secular equation.

It is shown in the Appendix of Reference 4 that the power travelling to the right is

$$P^+ = \frac{1}{2} \frac{\omega}{k} \mu_o |h_x|^2 \frac{\partial}{\partial k} (\mu^{sn} - \mu^{sp}),$$

where h_x and μ^s are found in the same plane. On using Eq. (A4) to obtain $h_x - ib_y/\mu_o\mu^s$, we obtain

$$P^+ = \frac{1}{2} \mu_o \omega (j_2 + rj_1)^2 K^+, \tag{A5}$$

in which K^+ is a coupling constant,

$$K^+ = (\mu^s(0))^2/k \frac{\partial}{\partial k} [\mu^{sn}(0) - \mu^{sp}(0)]. \tag{A6}$$

This definition differs by a factor of two from that used in Reference 4, because there are two films (see below).

Symmetric System. For two equal films with $\mu_{12} = 0$, text Eq. (15) is, at the roots of the secular equation,

$$\mu^s(0) = \tanh \frac{1}{2} kt, \text{ (even modes)},$$

$$\coth \frac{1}{2} kt, \text{ (odd modes)},$$

From Eq. (A3) we find $r = \pm 1$ for even and odd modes. The total power radiated in the positive direction is the sum of powers in even and odd modes

$$P^+ = \frac{1}{2} \mu_o \omega \left[(j_2 + j_1)^2 K_e^+ + (j_2 - j_1)^2 K_o^+\right] \tag{A7}$$

Note that, for widely separated films and $j_1 = 0$, only the lower film is excited and $K_e^+ \simeq K_o^+ = K^+$. The radiated power is then $P^+ = \mu_o \omega j_2^2 K^+$, which agrees with the definition in Reference 4 for coupling to a single film.

The permeabilities in Eq. (A6) are given in text Eqs. (11) and (13). Evaluation in the case of a symmetric system without a ground plane gives

$$K^+ = \mu_{22} k^{-1} \left[2d + \mu_{22} t - \mu_{22} (2d \mu_{11} + t)(\mu^s(0))^{-2}\right]^{-1}. \tag{A8}$$

This form holds equally for odd and even modes.

Exterior Currents

When the current sheets lie outside the magnetic films, as in Figure 7(c), an extension of the above argument yields a power dissipation similar to that in Eq. (A7), except that the coupling constants are multiplied by a numerical factor

$$K^+_{\text{exterior}} = K^+ \left[1 - \mu_{11}\mu_{22} (\mu^s(0))^{-2}\right] \left[1 - \mu_{11}\mu_{22}\right]^{-1}. \tag{A9}$$

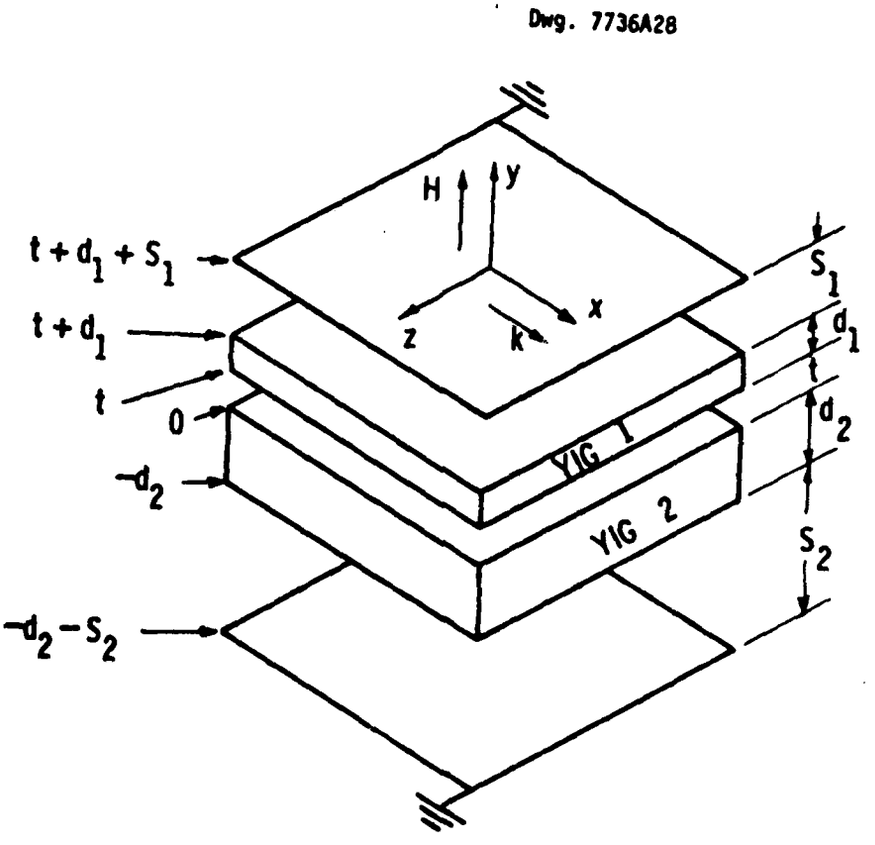

Fig. 1 Double YIG film configuration; the direction of H allows propagation of FVWs.

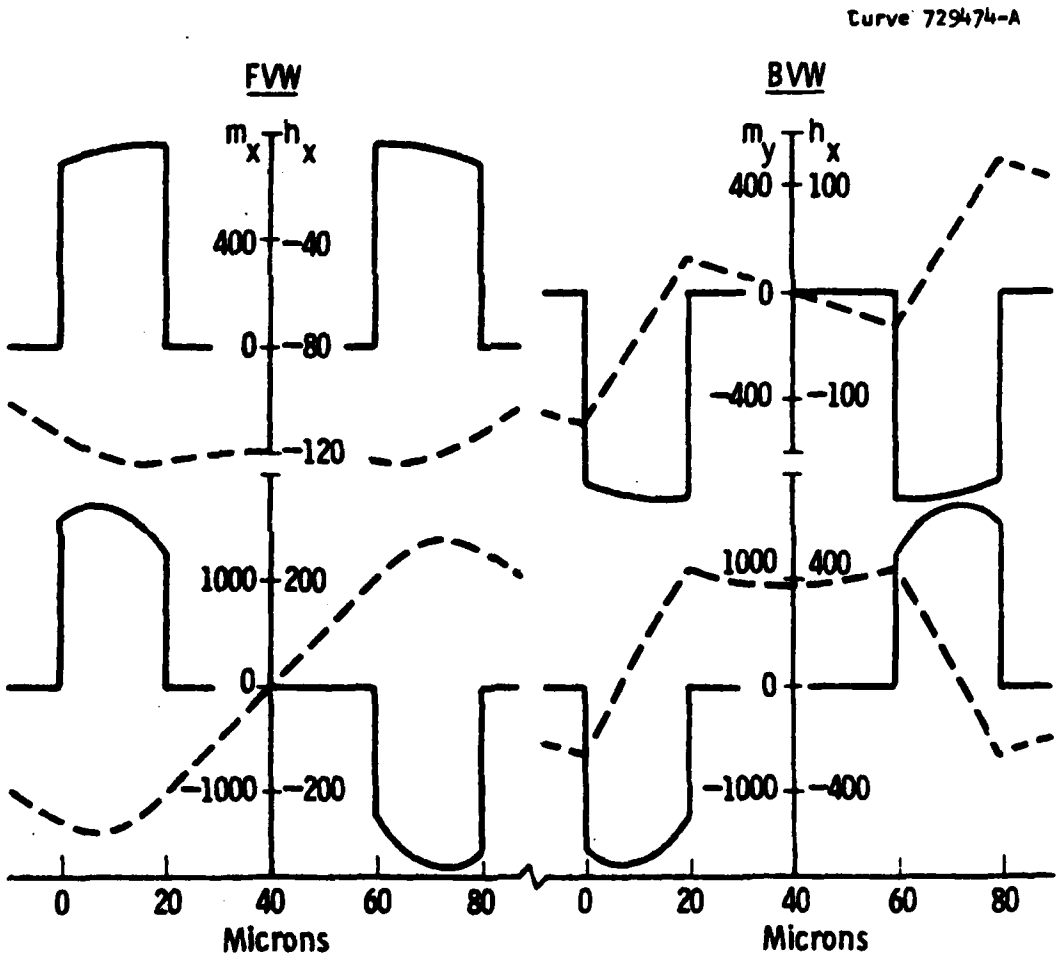

Fig. 2 The rf components of magnetization (m_x, m_y ——) and field (h_x ——) as a function of distance normal to the plane of two 20 micron thick films spaced 40 micron apart: L.H. curves - FVWs (f = 9.4 GHz, k_S = 112.93 cm^{-1}, k_A = 256.75 cm^{-1}); R.H. curves - BVWs (f = 10.25 GH_z, k_S = 122.83 cm^{-1}, kA = 268.84 cm^{-1}).

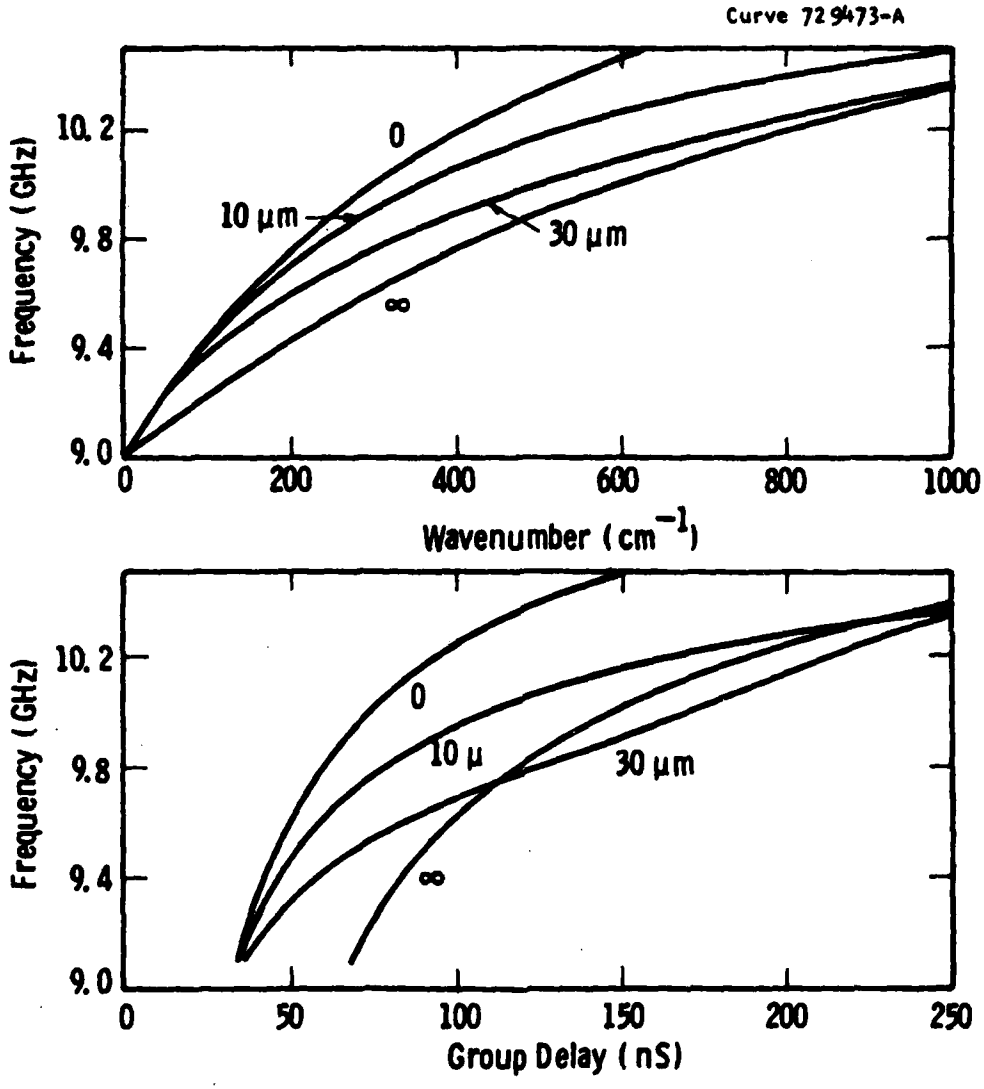

Fig. 3 The dispersion and group delay curves for a symmetric FVW propagating in two 20 micron thick films with the film separation (t) as a parameter; $4\pi M_1 = 4\pi M_2 = 1.8$ kG, H = 3.214 kG, $S_1 = S_2 = 1$cm.

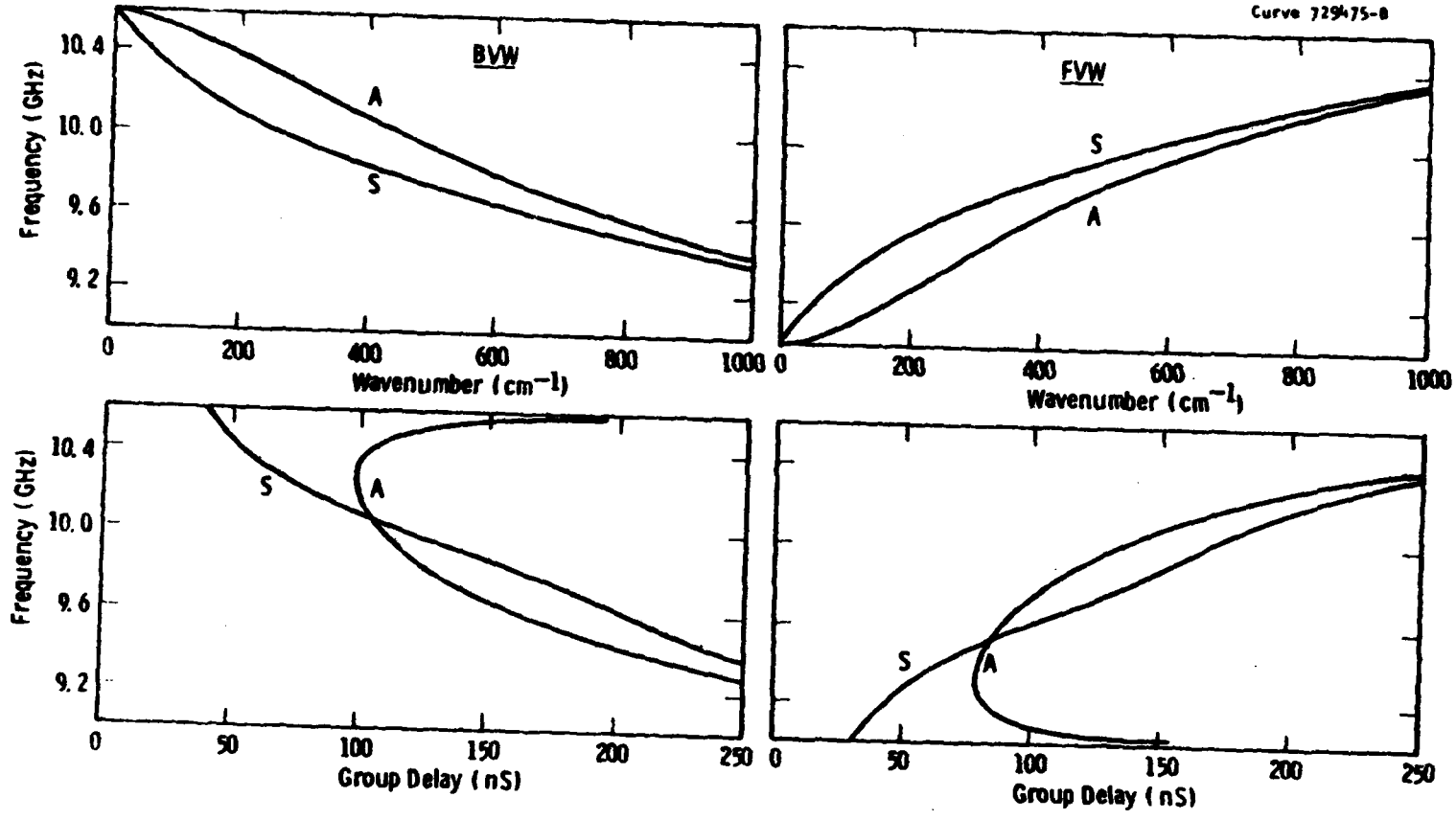

Fig. 4 The dispersion and group delay curves for FVWs and BVWs propagating in 20 micron thick films separated by 40 microns. The differences between the symmetric (S) and antisymmetric (A) modes are illustrated; other parameters as in Fig. 3 except H_{BVW} = 2.991 kG, t_{BVW} = 30 microns, t_{FVW} = 40 microns.

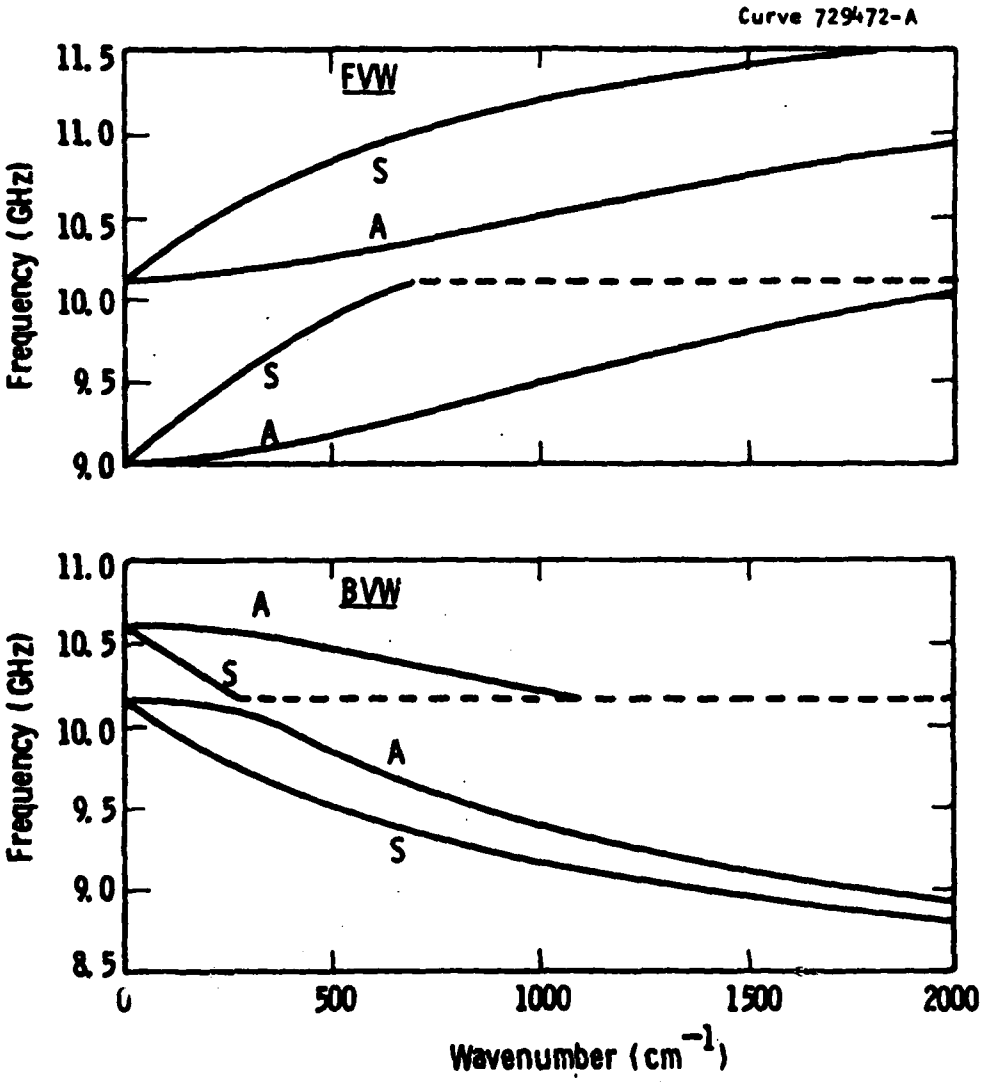

Fig. 5 The dispersion curves for FVWs and BVWs propagating in films of equal thickness but different magnetizations; $4\pi M_1$ = 1.8 kG, $4\pi M_2$ = 1.4 kG, t = 40 microns, $S_1 = S_2$ = 1cm, H_{FVW} (in film #1) = 3.214 kG, H_{BVW} = 2.991 kG.

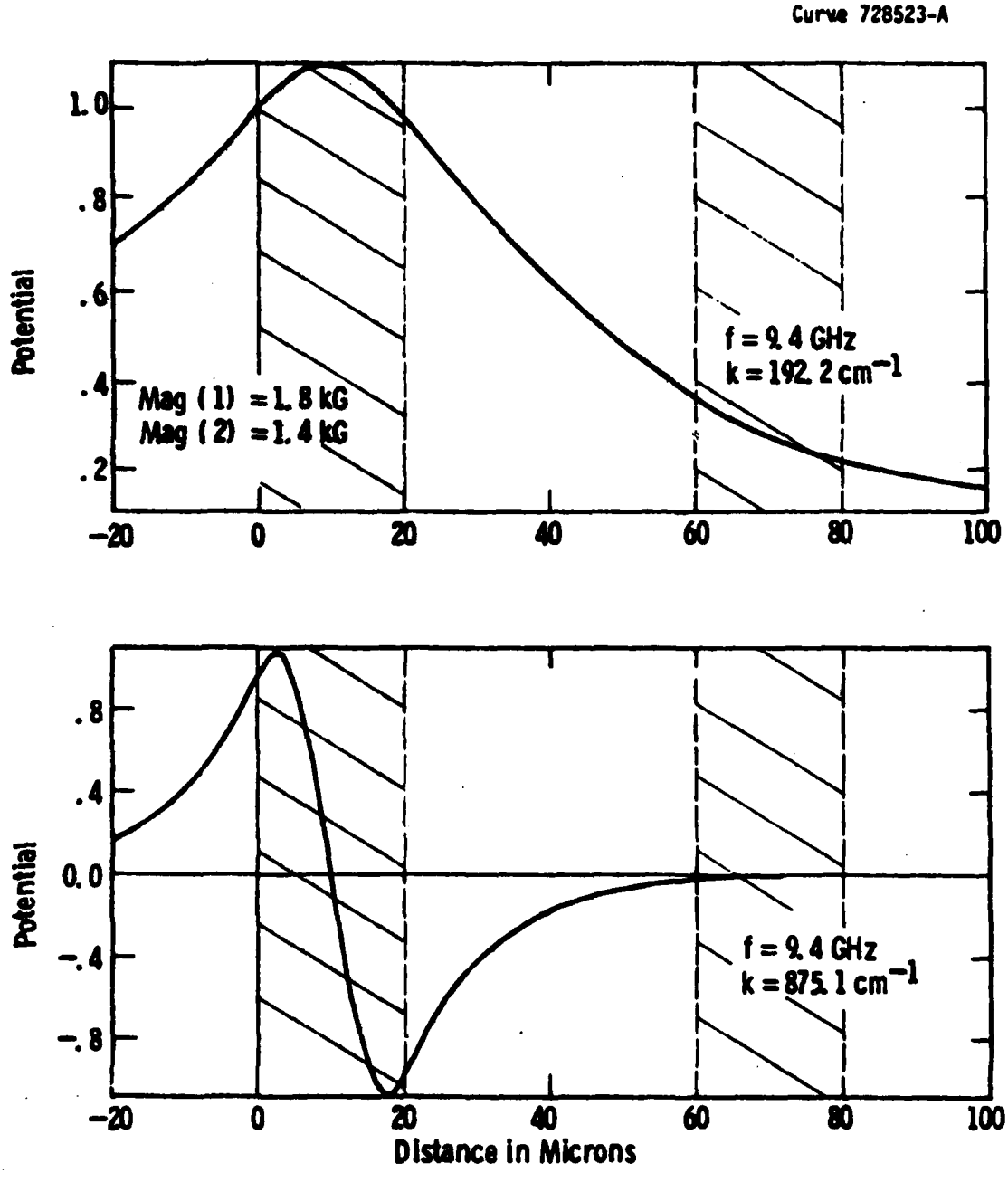

Fig. 6 The magnetostatic potential as a function of distance normal to the plane of two 20 micron thick films spaced 40 microns apart supporting a FVW: upper curve the first or fundamental mode; lower curve the first overtone.

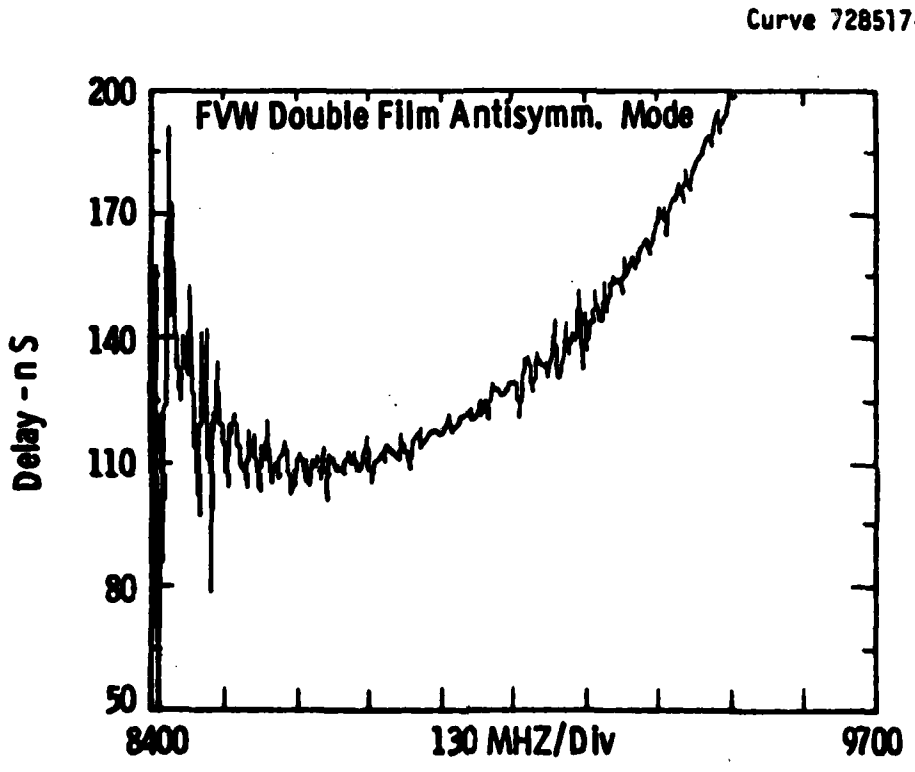

Fig. 8 Experimental results of group delay versus frequency for a FVW A-mode in two 20 micron thick YIG films spaced 25 microns apart.

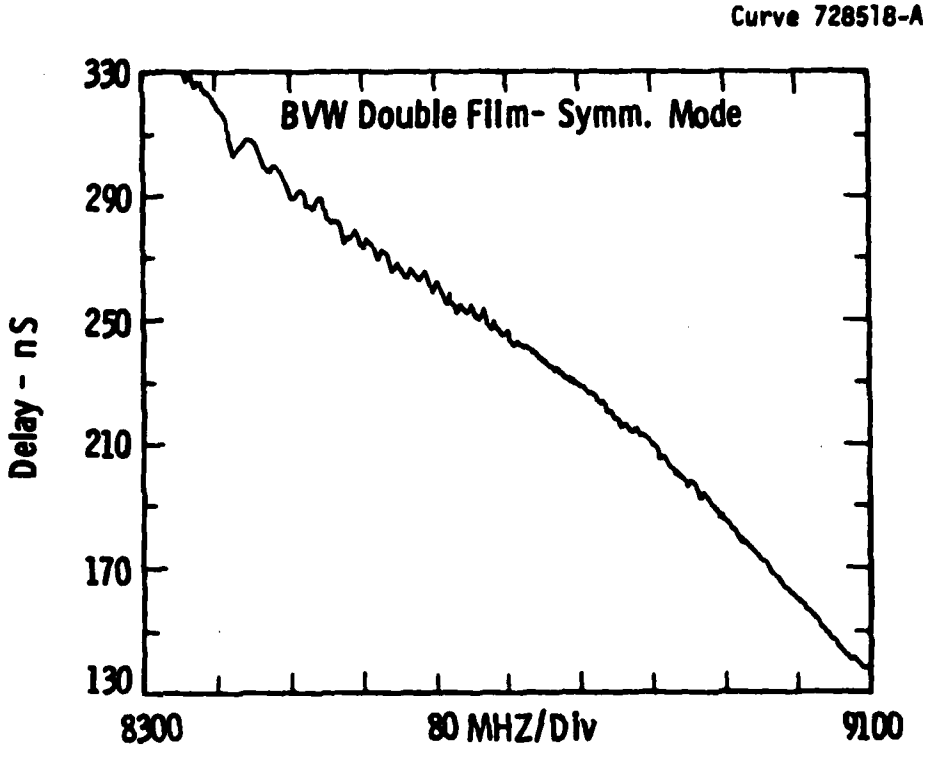

Fig. 9 Experimental results of group delay versus frequency for a BVW S-mode in two 20 micron thick YIG films spaced 25 microns apart.

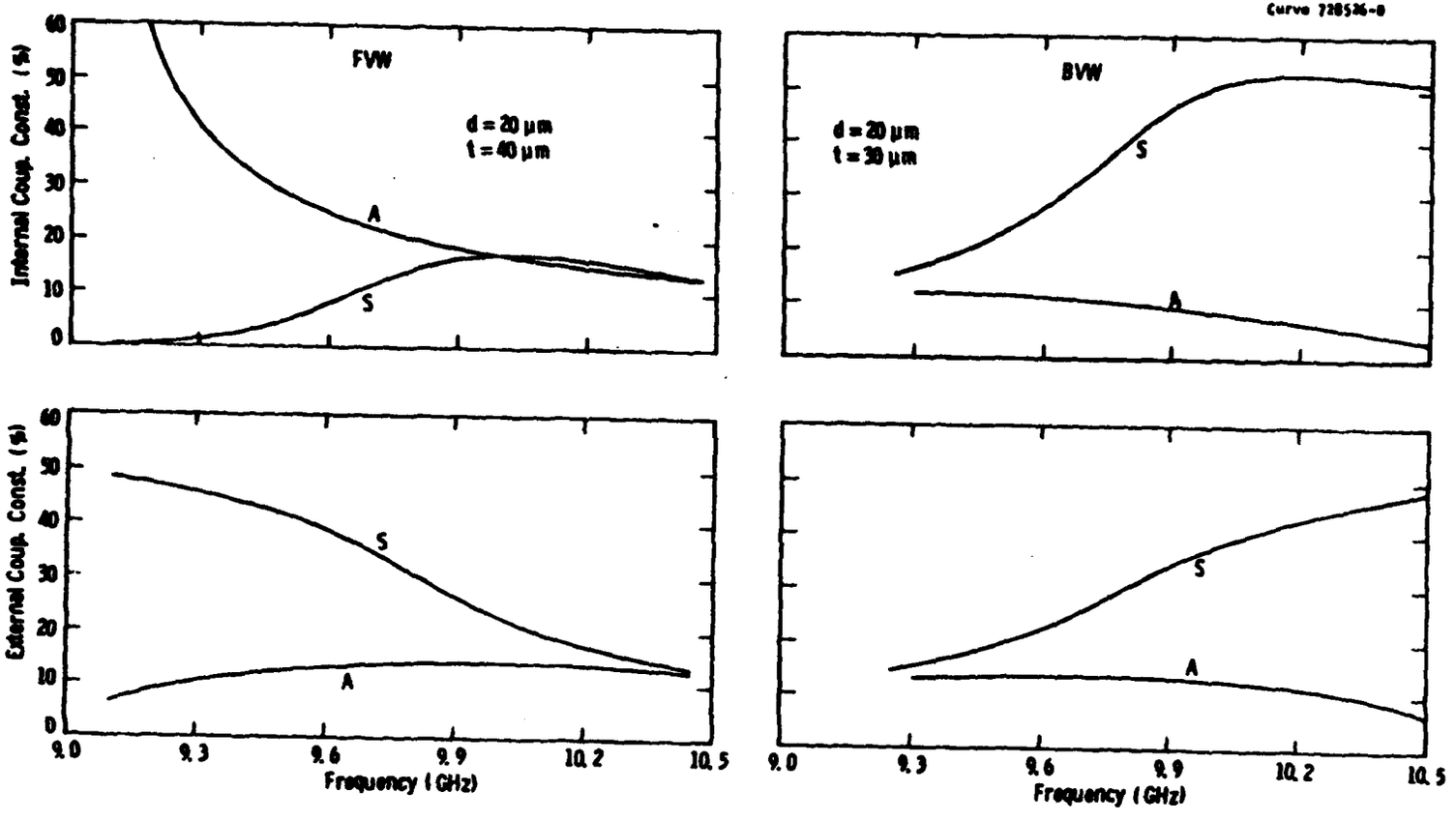

Fig. 11 The coupling constants as a function of frequency for the excitation of FVW and BVW S- and A-modes in two 20 micron thick films; $4\pi M_1 = 4\pi M_2 = 1.8$ kG, $H_{FVW} = 3.214$ kG, $H_{BVW} = 2.991$ kG, S_1 and $S_2 \rightarrow \pm =$ respectively

APPENDIX B

MAGNETOSTATIC DELAY LINES* USING YIG DOUBLE FILMS

Michael R. Daniel and J. D. Adam
Westinghouse Electric Corporation
R&D Center
Pittsburgh, PA 15235

ABSTRACT

Magnetostatic volume waves propagating in YIG double films offer the potential of microwave delay lines with either linearly dispersive or nondispersive delay characteristics. This is achieved without the need for nearby ground planes and their concomitant attenuation of the magnetostatic waves. Two modes of propagation are identified in double films from the symmetry of the rf magnetization or magnetic field. Conventional transducers can excite either mode and care may be needed to avoid exciting them simultaneously in some geometries.

1. INTRODUCTION

At this conference two years ago, we described how magnetostatic waves propagating in an yttrium iron garnet film (YIG) could be made to exhibit a delay versus frequency characteristic which was almost linear over about 1 GHz of bandwidth.[1] This was achieved through the influence of a close proximity ground plane on the dispersive behavior of the waves. However, one penalty to be paid for this approach to linearizing the delay is an increased insertion loss due to eddy current damping of the magnetostatic wave by the finite conductivity ground plane.[2] We were thus motivated to see whether magnetostatic waves propagating in two films coupled by their close proximity offered any useful delay characteristics without the concomitant ground plan damping. Some work on double films has already appeared in the literature of a mostly theoretical nature.[3-5]

*Work supported in part by U.S. Air Force (RADC) under Contract F19628-80-0150.

We shall be concerned with forward volume waves (FVWs) and backward volume waves (BVWs). Our approach to computing the dispersion of magnetostatic waves in a double film using the concept of "surface permeabilities" will be described elsewhere.[6] We may summarize the results of these calculations by saying that the dispersion relation yields two sets of solutions. These sets have been termed the symmetric (S) and antisymmetric (A) sets, respectively. The term S or A describes the symmetry of the rf magnetization (m) or rf field (h) normal to the bias field H. This is illustrated in Fig. 1 for FVWs where two possible transducer geometries are also shown which should excite either the S-mode (Fig. 1a) or the A-mode (Fig. 1b) for FVWs. However, because the magnetostatic waves are launched by h components normal to the bias field, the relevant fields for BVW propagation are the h-components normal to the plane of the YIG film. These components would have opposite symmetry to those shown in Fig. 1. Thus, the transducer configurations (a) and (b) will launch the BVW A-mode and S-modes, respectively. In what follows, we shall be concerned only with the lower order S- and A-modes. The higher order thickness modes were not observed in transmission loss measurements on double film delay lines.

2. RESULTS

2.1 Calculations

Fig. 2 shows that for an appropriate choice of film thickness (d) and film separation (t), both FVWs and BVWs can be made to exhibit either a linearly dispersive or a quasi-constant delay. The delay was calculated from the slope of the dispersion relation ($dk/d\omega$) and both films were assumed of equal magnetization ($4\pi M$). The film separations of 40 microns for the FVW and 30 microns for the BVW represent values which give optimum degrees of linearity over approximately 1 GHz of bandwidth for the 20 micron thick films supporting S-modes. The two curves for the A-modes each show a region of constant delay ($\pm$ 5 nS) over a bandwidth of 0.4 GHz. The deviation from linearity of the S-modes is shown in Fig. 3 where the phase deviation from a quadratic response is plotted as a function of frequency. These

results and those of Fig. 2 for the constant delay A-modes compare very favorably with what can be achieved using a single YIG film, except that for the double films there are no ground planes needed to achieve the results and hence, no extra transmission loss from ground plane damping of the magnetostatic waves.

2.2 Experiments

The experiments to be described here were performed on double YIG structures consisting of two 20 micron thick YIG strips cut from the same epitaxial film and separated by the thickness of the wire transducers similar to Fig. 1. The YIG films were grown by liquid phase epitaxy on gadolinium gallium garnet (GGG) substrates. The delay line measured 25 mm by 3 mm and in the first experiment the two films sandwiched single 25 μm diameter gold wires for the transmitter and receiver transducers. Thus, the rf field pattern was appropriate to Fig. 1b. However, for BVWs with the bias field, H, parallel to the propagation direction, the normal h fields are symmetric in both films. Thus, an S-mode would be expected and this is confirmed by the delay measurements of Fig. 4, which show the quasi-linear response. The results of Fig. 4 and subsequent results were taken on an automatic network analyzer (HP model 8410B) under computer control (HP model 9845B). The bias field was provided by a 12 in. Varian electromagnet. The results for FVWs shown in Fig. 5 were obtained with the same sample as described above, but with H normal to the film plane as shown in Fig. 1b. Hence, an A-mode was anticipated with a region of constant delay and this was obtained. The origin of the higher noise level on the delay results of Fig. 5 compared to Fig. 4 is presently unknown but is believed to be instrumental.

There was considerable interest to launch an S-mode for FVWs because of the potential for an "up-chirp" dispersive delay line. The double or "opposed" transducer arrangement of Fig. 1a was chosen for this by using gold ribbon transducers 50 microns by 12 microns in cross-section. The upper and lower elements of the transducers were kept apart by a film of commercial polymer (Saran-Wrap). The results of Fig. 6, unfortunately, suggest

that mainly A-mode was being launched. The high noise level on the delay results may have been in part a result of interference between the S- and A-modes. We note that the h-field components from the upper and lower elements of a double transducer will tend to cancel since the microwave currents in each element are in opposition to one another. Therefore, any asymmetry in the structure will tend to promote the A-mode at the expense of the S-mode. Evidently, strong h-field cancellation is occurring in Fig. 5. The essential correctness of this interpretation was borne out by the coupling constant calculation of Fig. 6. The details of this calculation are given in reference (6). For FVWs, the S-mode coupling is substantially weaker than the A-mode over most of the frequency range for the transducer geometry used here. In reference (6), it is shown that coupling to the YIG films with the transducer elements exterior to them and not interior as in Fig. 1a improves the S-mode coupling strength and weakens the A-mode coupling. To take advantage of this requires a compositely grown double YIG structure without the 500 micron thick GGG substrates. The GGG would form a thin epitaxial spacer between the films.

3. CONCLUSIONS

We have shown that FV- and BV- magnetostatic waves propagating in a YIG double film structure offer the potential for both dispersive and nondispersive delay lines with bandwidths of 1 GHz and 0.4 GHz, respectively. This has been achieved without the use of ground planes and thus, lower insertion losses are predicted compared to those obtainable from single YIG film delay lines. The double film structures do support two types of magnetostatic wave and some care may have to be exercised in transducer design so as not to excite the undesired mode in a particular situation.

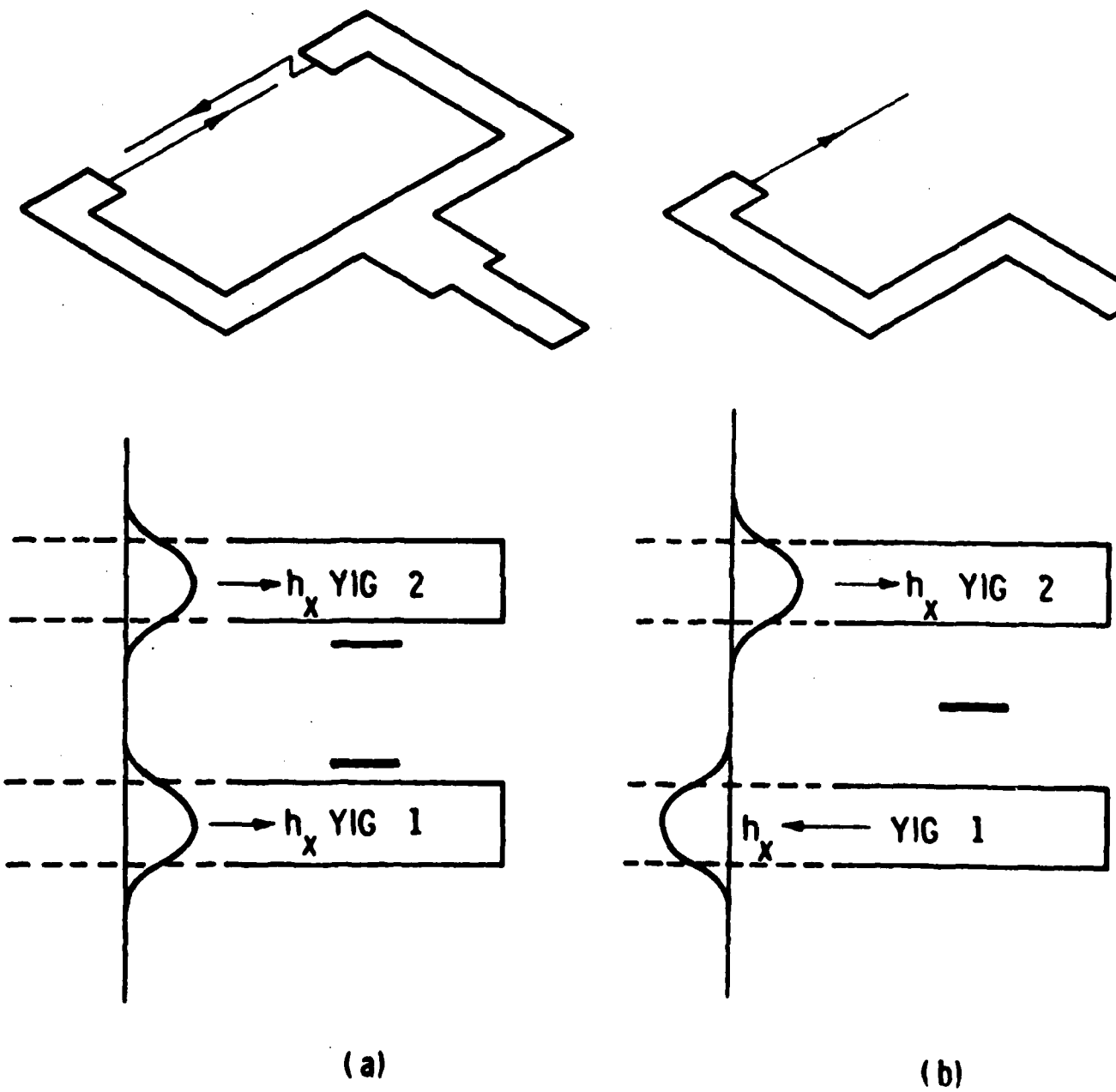

Figure 1 Possible transducer configurations and rf field patterns for a FVW symmetric mode (a) and antisymmetric mode (b). The static bias field is normal to the plane of the YIG films.

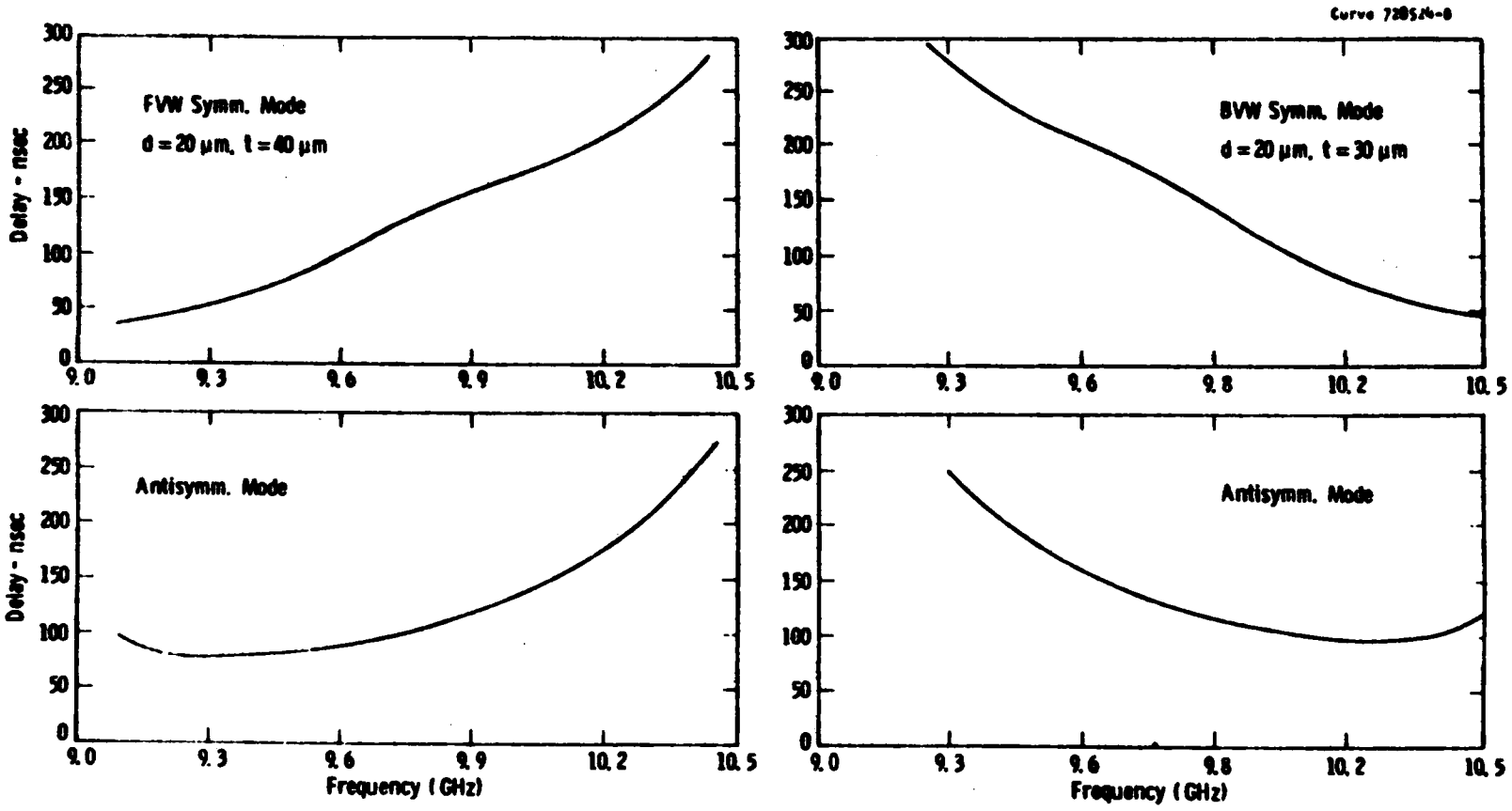

Figure 2 Calculated delay versus frequency for both S- and A-modes of FVWs and BVWs which show an optimum degree of delay linearity for the S-modes.

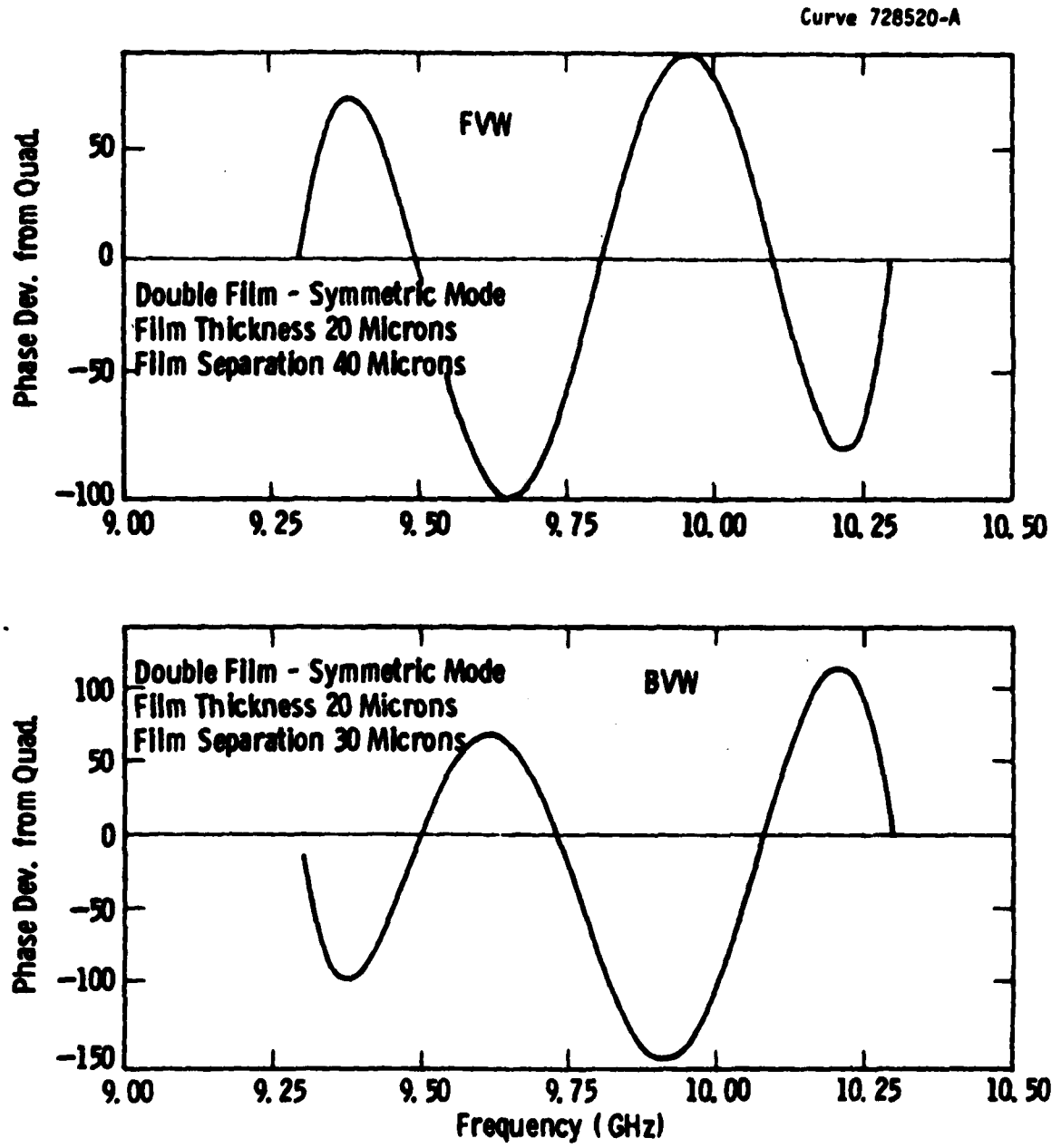

Figure 3 Phase deviation from ideal quadratic response versus frequency for the two S-mode responses shown in Fig. 2.

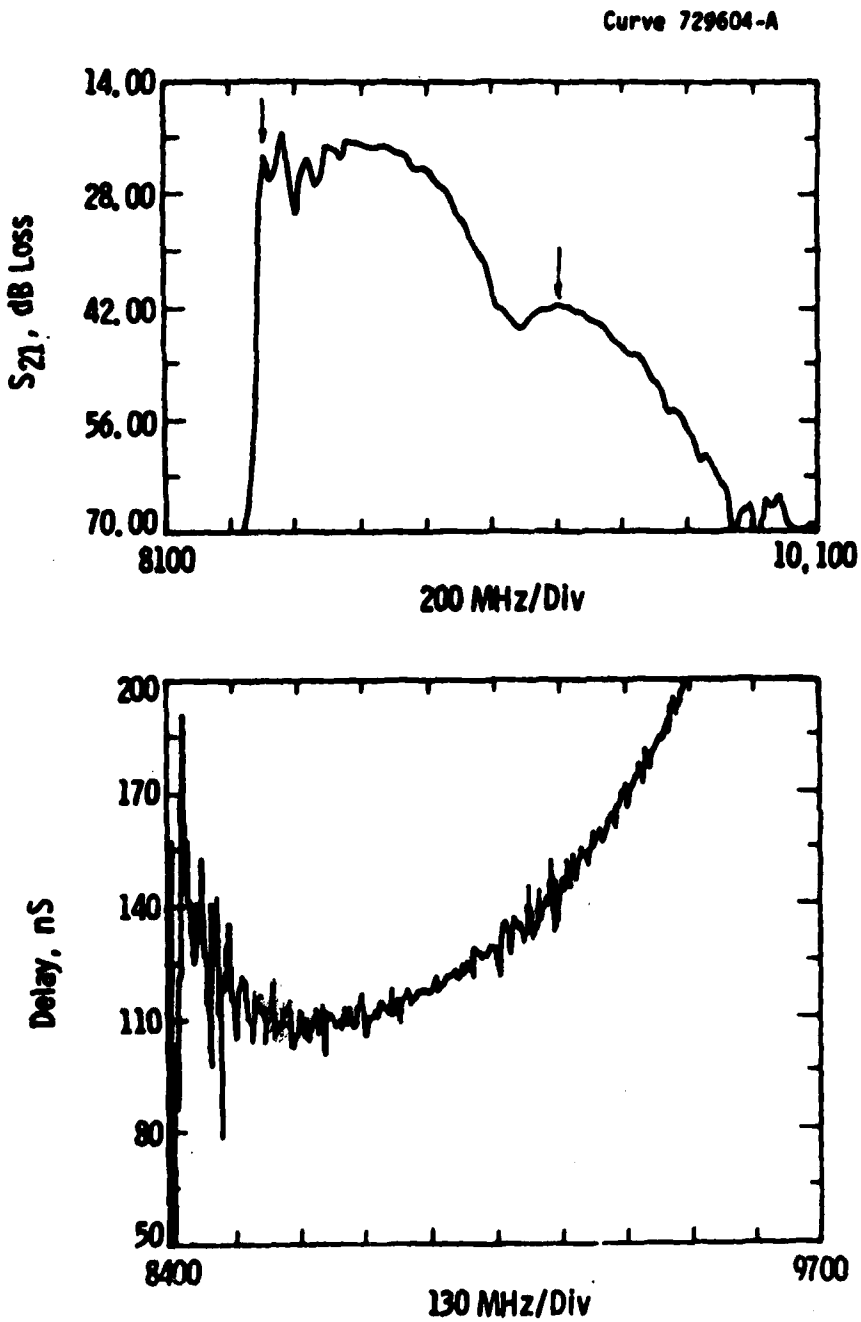

Figure 5 Network analyzer responses for a FVW A-mode propagating in two 20 micron thick YIG films separated by 25 microns: upper curve -- transmission parameter, S_{21}, versus frequency; lower curve -- group delay versus frequency. Arrows in the upper curve define interval over which the group delay results were measured.

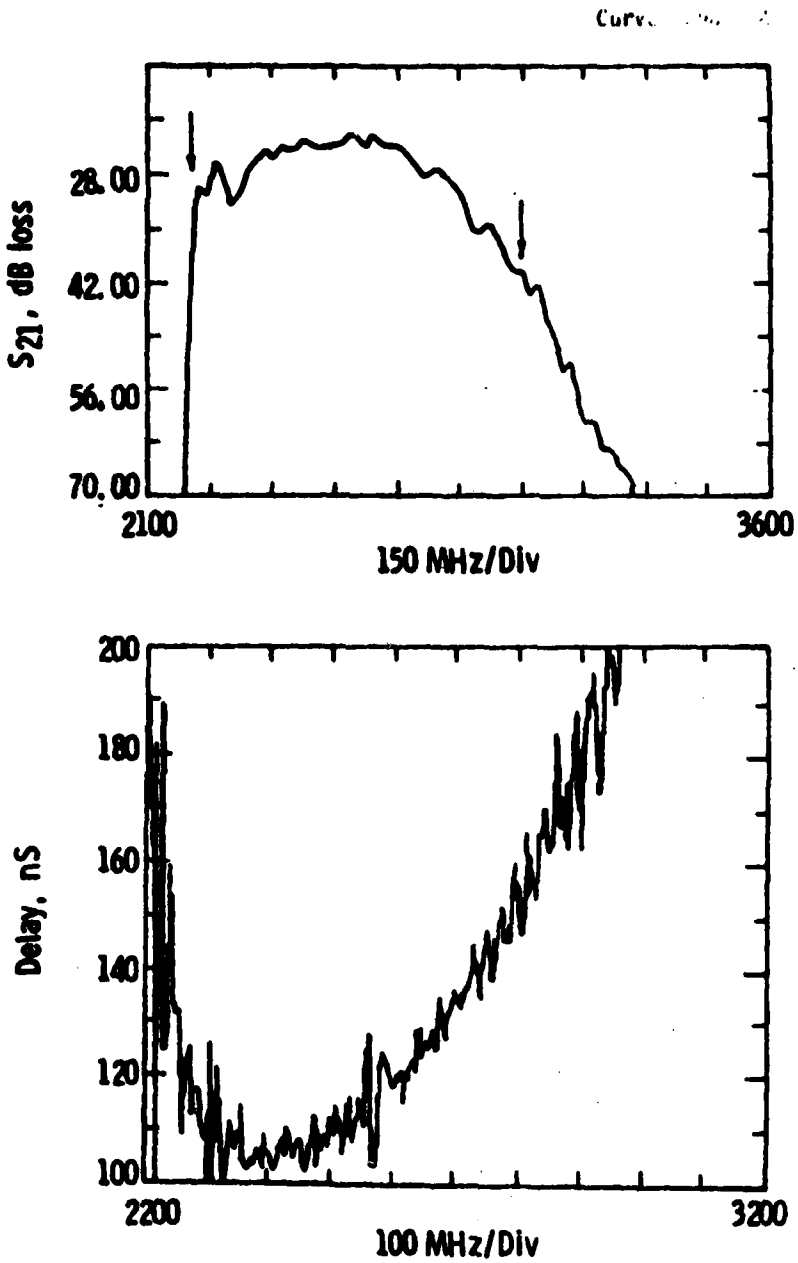

Figure 6 Network analyzer responses for a FVW propagating in two 20 micron thick YIG films separated by approximately 40 microns: upper curve -- transmission parameter, S_{21}, versus frequency; lower curve -- group delay versus frequency. Arrows in the upper curve define interval over which the group delay results were measured.

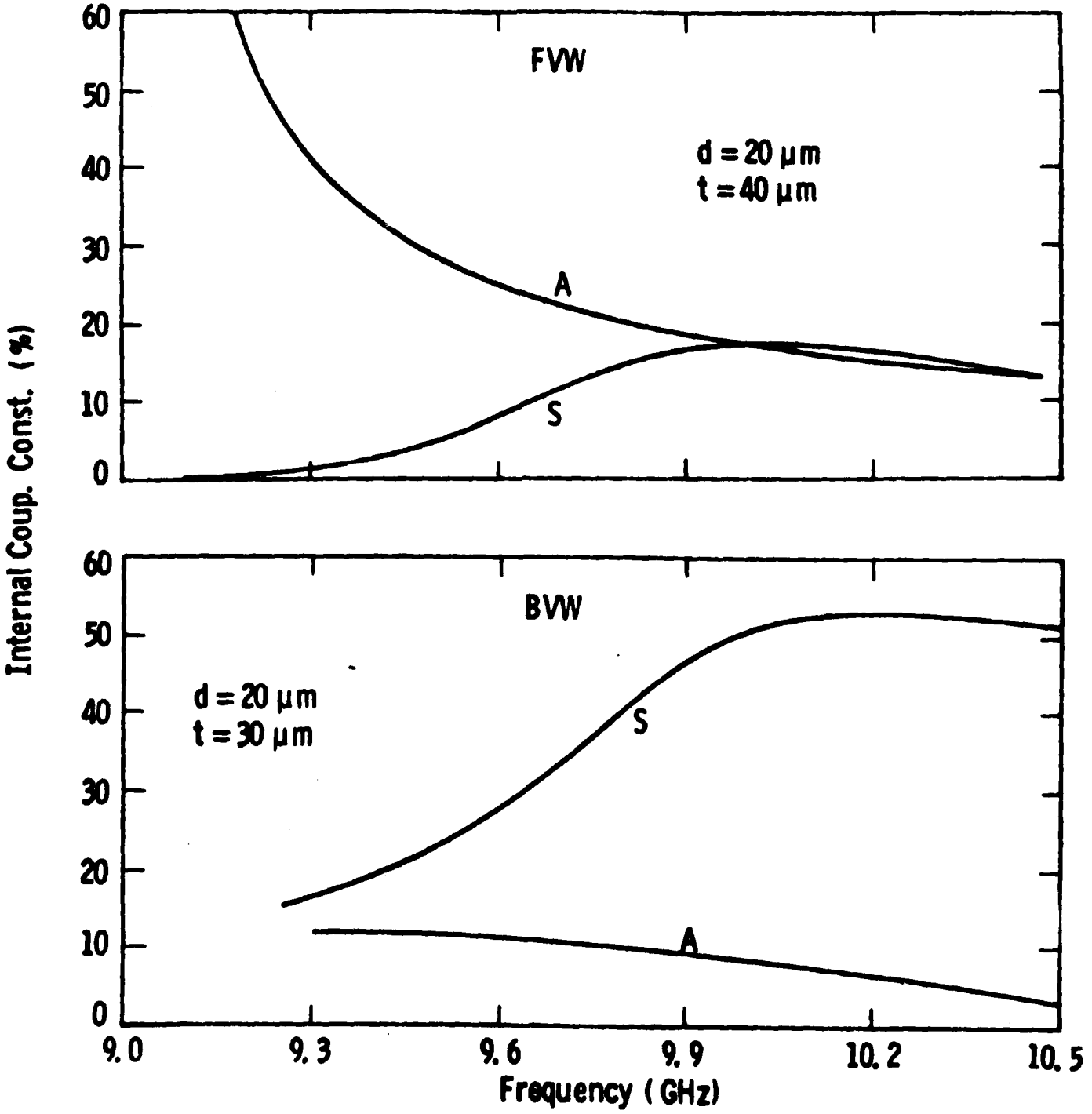

Figure 7 Calculated coupling coefficients in percent versus frequency for FVWs and BVWs using the transducer geometry of Fig. 1a.

END

FILMED